Transportation Research Part C 85 (2017) 86–110

Contents lists available at ScienceDirect

Transportation Research Part C

journal homepage: www.elsevier.com/locate/trc

Closed-form multiclass cell transmission model enhanced with overtaking, lane-changing, and first-in first-out properties

Kamonthep Tiaprasert [a,*], Yunlong Zhang [b], Chaodit Aswakul [c], Jian Jiao [b], Xin Ye [a]

[a] Key Laboratory of Road and Traffic Engineering of Ministry of Education, College of Transportation Engineering, Tongji University, Shanghai 201804, China
[b] Zachry Department of Civil Engineering, Texas A&M University, College Station, TX 77840, United States
[c] Wireless Network and Future Internet Research Unit, Department of Electrical Engineering, Faculty of Engineering, Chulalongkorn University, Bangkok 10330, Thailand

ARTICLE INFO

Article history:
Received 15 March 2017
Received in revised form 10 September 2017
Accepted 10 September 2017

Keywords:
Traffic flow theory
Multiclass macroscopic modeling
Cell transmission model
Heterogeneous mobility
Traffic network

ABSTRACT

A novel multiclass macroscopic model is proposed in this article. In order to enhance first-in, first-out property (FIFO) and transmission function in the multiclass traffic modeling, a new multiclass cell transmission model with FIFO property (herein called FM-CTM) is extended from its prior multiclass cell transmission model (M-CTM). Also, to enhance its analytical compactness and resultant computational convenience, FM-CTM is formulated in this paper as a set of closed-form matrix equations. The objective is to improve the accuracy of traffic state estimation by enforcing FIFO property when a fast vehicle cannot overtake a slow vehicle due to a limitation of a single-lane road. Moreover, the proposed model takes into account a different priority for vehicles of each class to move forward through congested road conditions, and that makes the flow calculation independent from their free-flow speeds. Some hypothetical and real-world freeway networks with a constant or varying number of lanes are selected to verify FM-CTM by comparing with M-CTM and the conventional CTM. Observed densities of VISSIM and real-world dataset of I-80 are selected to compare with the simulated densities from the three CTMs. The numerical results show that FM-CTM outperforms the other two models by 15% of accuracy measures in most cases. Therefore, the proposed model is expected to be well applicable to the road network with a mixed traffic and varying number of lanes.

1. Introduction

Traffic state estimation, dynamic traffic assignment, and dynamic traffic flow models have been developed over the years as an important component in real-time traffic management. Since real-time applications require computational efficiency, macroscopic models are essentially applied in those situations. For macroscopic modeling and its extensions, a good review can be seen in the following literature (Mohan and Ramadurai, 2013; Castillo et al., 2015). LWR (Lighthill, Whitham, and Richards) model, (Lighthill and Whitham, 1955; Richards, 1956), is considered the first macroscopic model of this type.

Cell transmission model (CTM) proposed by Daganzo (Daganzo, 1994, 1995) is one of the most well-known discretized versions of LWR model. Since its first inception, CTM has been widely extended and used in a number of transportation

* Corresponding author.
E-mail addresses: kamonthep.t@gmail.com (K. Tiaprasert), yzhang@civil.tamu.edu (Y. Zhang), chaodit.a@chula.ac.th (C. Aswakul), jiaojian@tamu.edu (J. Jiao), xye@tongji.edu.cn (X. Ye).

http://dx.doi.org/10.1016/j.trc.2017.09.008
0968-090X/

applications. For instance, to take into account a random fundamental diagram, stochastic CTM was proposed by Alecsandru (2006), Boel and Mihaylova (2006), Zhong and Sumalee (2008), Sumalee et al. (2011). Stochastic CTM for urban networks was proposed by Hadfi et al. (2017). The extension of CTM with variable speed limits was proposed by Han et al. (2017). With the emergence of probe and autonomous vehicles, a velocity-CTM (Work et al., 2008) was studied to estimate time-varying traffic density directly from obtainable speed data. Levin and Boyles (2016a) applied CTM to simulate the overall behavior of autonomous vehicles with dynamic lane reversal. In an attempt to explain lane-changing behavior, CTM was also extended to enable lane-changing property (Laval and Daganzo, 2006; Carey et al., 2015). To emphasize on ramp metering control, Gomes and Horowitz (2006), Gomes et al. (2008) explained and studied ramp metering phenomena with CTM. In addition, Flötteröd and Nagel (2005) extended CTM to simulate more-than-two-upstream and/or -downstream cells directly with a connector.

To track dynamic traffic flow patterns, CTM with a neural network theory or with a fuzzy c-means clustering were proposed by Celikoglu and Silgu (2016), Celikoglu (2014), Silgu and Celikoglu (2015), Celikoglu (2013). Lu et al. (2011) extended the lagged cell-transmission model (Daganzo, 1999) to capture the dynamics of density and the probability distribution of vehicle velocity concurrently. In addition, CTM finds its applications in signal optimization, dynamic traffic assignment, and evacuation planning (Lo et al., 2001; Szeto, 2008; Ukkusuri and Waller, 2008; Kalafatas and Peeta, 2010; Zhang et al., 2013; Zhu et al., 2013; Zhang et al., 2015). Though CTM has the advantages of fast computational time, queue accumulation and spillback prediction accuracy as well as usefulness applicability towards large-scale road networks, CTM assumes that a flow can be captured well by only one velocity average, i.e. a free-flow speed. As a result, CTM in its original forms has still a limitation in abstracting such realistic phenomena as those related to traffic heterogeneities, commonly found in practical urban and highway roads with multiple vehicle types.

In that regard, researchers have in the past tried to address the heterogeneous traffic behavior. To produce platoon dispersion phenomena, LWR was extended to multiclass LWR (Wong and Wong, 2002). The model introduces the notion of classes defined heterogeneous driving on a freeway. In general, as heavy vehicles (HVs) require larger space and have less mobility (free-flow speed) than passenger vehicles (PVs), multiclass models were developed for a freeway with high percentage of HVs with the objective of dynamic traffic assignment or traffic state estimation (Ngoduy and Liu, 2007; Van Lint et al., 2008; Ngoduy, 2011; Szeto et al., 2011; Mesa-Arango and Ukkusuri, 2014; Liu et al., 2015; Qian et al., 2017; Zhan and Ukkusuri, 2017). In addition, an extension was also developed for PVs and buses in an urban area for a bus-rapid transit system (Liu et al., 2015). Freeway and highway multiclass models have been applied to evaluate how HVs can affect overall traffic flow. On the other hand, the distinct behaviors of buses and PVs are of interest to traffic signal control problems considering a bus priority. With the advent of connected and autonomous vehicles, CTM was extended to model a mixed traffic of human and autonomous vehicles (Levin and Boyles, 2016b).

In order to produce platoon dispersion in a general topology, CTM was extended to multiclass CTM by Tuerprasert and Aswakul (2010). The prior multiclass CTM, denoted as M-CTM, was compared with the conventional CTM, denoted as S-CTM, and with a microscopic simulator. Based on the reported results, M-CTM is found be able to produce platoon dispersion well without compromising on the model's computational complexity. As a sequel, in this article, M-CTM is further enhanced and generalized to model the scenario of heterogeneous lanes and with first-in, first-out (FIFO) property. Here, the proposed model is named FM-CTM, standing for the multiclass cell transmission model with FIFO property. FIFO can occur with traffic congestion or in a single lane with or without multiclass traffics. To the best of authors' knowledge, there is no multiclass macroscopic model that can well quantify the impact of the number of lanes on the model performance as most researchers have only verified their traffic flow models with constant-lane homogeneous roads. Moreover, FM-CTM considers that a vehicle with a low free-flow speed could occasionally move ahead of the one with a high free-flow speed during traffic congestion by outmaneuvering aggressiveness or by its movement flexibility due to a compact size (Nair et al., 2011). In overall, FM-CTM in this paper aims to enhance the existing M-CTM by introducing the following newly contributed features;

1 Multiclass traffic state estimation when an overtaking is unavailable and hence the FIFO property of resultant flow.
2 Transmission model enhancement to mimic the behaviors of slow vehicles during free-flow condition.
3 Overtaking model independent of the free-flow speed for a congested road condition.

In addition to these new features, unlike the prior work of M-CTM (Tuerprasert and Aswakul, 2010), FM-CTM is formulated as a set of closed-form matrix equations. This closed-form matrix derivation finds applications in a feedback control theory as desirable observability and controllability are conveniently obtainable. Further, computer programming for the model computability can be numerically facilitated with matrix, instead of scalar, equations. For instance, all the codes of FM-CTM have been developed in Matlab in this research.

This paper is organized as follows: firstly, FM-CTM is proposed along with the closed-form matrix formulation in Section 2. Secondly, the theoretical proof to validate FM-CTM's convergence to the single-class LWR model is elaborated in Section 3. Numerical results comparing the new and old M-CTM are given in Section 4. Finally, Section 5 presents conclusions and future work.

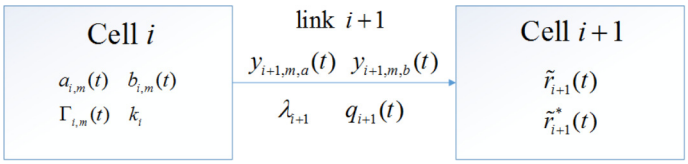

Fig. 1. Cell cascading connection and its associate parameters and indexes.

2. Multiclass cell transmission model with heterogeneous lanes and FIFO properties

This section presents the formulation for FM-CTM in cascading scenario as depicted in Fig. 1. There are three important assumptions for FM-CTM. The first two assumptions were used by M-CTM as well, whereas the third assumption is the new assumption for FM-CTM. The first assumption is that the fastest vehicle class has the free-flow speed no greater than two times as much as the slowest vehicle. Hence, the normalized free-flow speed with respect to the fastest class (class-1) $\tilde{v}_m$ is between 0.5 and 1 with $\tilde{v}_1 = 1$. The second assumption is that the ratio of backward to forward wave propagation is assumed to be constant regardless of class index. Each class may not have the same forward and backward wave propagation speed, but we assume that the proportion of the two speeds is constant. By this assumption, the wave propagation ratio δ_i is insensitive to class index. The third assumption is that a traffic congestion experienced by end-of-cell vehicle of upstream cell is determined from a congestion level of its cell. End-of-cell vehicle is a vehicle that just enters its current cell in previous time slot, and they most likely are not at the head of the cell. Therefore, in contrast to head-of-cell vehicle and S-CTM, most perceived congestion and overtaking are determined by the traffic congestion level in the upstream cell rather than the downstream cell.

Class-1 vehicle denotes the vehicle class with the highest free-flow speed. The cell length is equal to the distance that the class-1 vehicle can travel during the free-flow condition which is time slot interval multiplied by the fastest class's free-flow speed. Then a straight road is divided into a cascading of cells with the uniform cell length. The effective length of class-m vehicle l_m is a vehicle length plus a minimum gap with the front vehicle, obtained through parameter calibration. The normalized vehicle length of class-m vehicle $\tilde{l}_m$ is equal to l_m/l_1 with $\tilde{l}_1 = 1$. The cell capacity c_i is equal to the cell length multiplied and divided by the number of lanes and the effective length of class-1 vehicle l_1, respectively.

The relative receiving capability of cell $i+1$ at time slot t is calculated from Eq. (1)

$$\tilde{r}_{i+1}(t) = \min\left\{ q_{i+1}(t), \delta_{i+1}\left(c_{i+1} - \sum_{m=1}^{M}\left(\tilde{l}_m \psi_{i+1,m}(t) n_{i+1,m}(t)\right)\right)\right\} \tag{1}$$

where $\tilde{r}_{i+1}$ is the relative receiving capability of downstream cell $i+1$ at time slot t. The relative occupancy ratio of class-m vehicles $\psi_{i+1,m}$ is a ratio of class-m to class-1 occupancy. The relative occupancy ratio of class-m vehicles takes into account as a slow vehicle tends to dwell in cell longer than a fast vehicle during one time slot frame. As traffic becomes more congested, the difference in mobility between slow and fast vehicles decreases. Thus, $\psi_{i+1,m}(t)$ converges to 1 as the density increases. There is no specific way to define $\psi_{i+1,m}(t)$ as it can be defined freely to reflect the condition in the real world. q_{i+1} is the maximum flow capacity of link $i+1$ at time slot t. $n_{i+1,m}$ is the total number of class-m vehicles of cell $i+1$ at time slot t and equal to head-of-cell plus end-of-cell vehicles of class-m of cell $i+1$ at time slot t.

Similar to M-CTM, FM-CTM divides vehicle flow for each class into two types, namely, head-of-cell and end-of-cell vehicles. Head-of-cell vehicle is defined as a vehicle that cannot move forward to the designated cell in the previous time slot, so it is assumed to be at the head of cell. Hence, all head-of-cell vehicles are ready to move to the next cell if there is a sufficient receiving capability. End-of-cell vehicle is defined as a vehicle that just enters a current cell in the previous time slot, so it is unable to move to the next cell in one time slot if its free-flow speed is lower than the free-flow speed of class-1 vehicle.

Then the closed-form matrix equations of FM-CTM are presented.

Fig. 2 and Table 1 give an overview on the formulation of FM-CTM versus M-CTM and S-CTM where $\Gamma_{i,m}$ is the transmission factor of class-m of cell i at time slot t, $\lambda_{i+1,m}$ is the overtaking factor of class-m head-of-cell vehicles on link $i+1$, and k_i is the ratio of congested density to the cell capacity of cell i. In FM-CTM's formulation, the transmission and overtaking abilities of each class are not only affected by their free-flow speed but the traffic condition as well. The transmission factor for M-CTM is equal to $\tilde{v}_m$, regardless of traffic condition or other vehicle classes in the same cell. On the other hand, FM-CTM calculates the transmission factor based on traffic condition and a mixture of vehicle classes. This allows FM-CTM to calculate the flow when overtaking is not available. Moreover, the transmission factor calculation for free-flow condition of slow vehicles is enhanced from M-CTM. In addition, the overtaking factor in FM-CTM is independent from free-flow speed to reflect that a slow but nimble vehicle may overtake a fast vehicle in congested condition. The ratio of congested density to the cell capacity is to identify the traffic condition of the cell to calculate the flow accordingly. In summary, FM-CTM is an extension of M-CTM with overtaking, lane-changing, and first-in first-out properties.

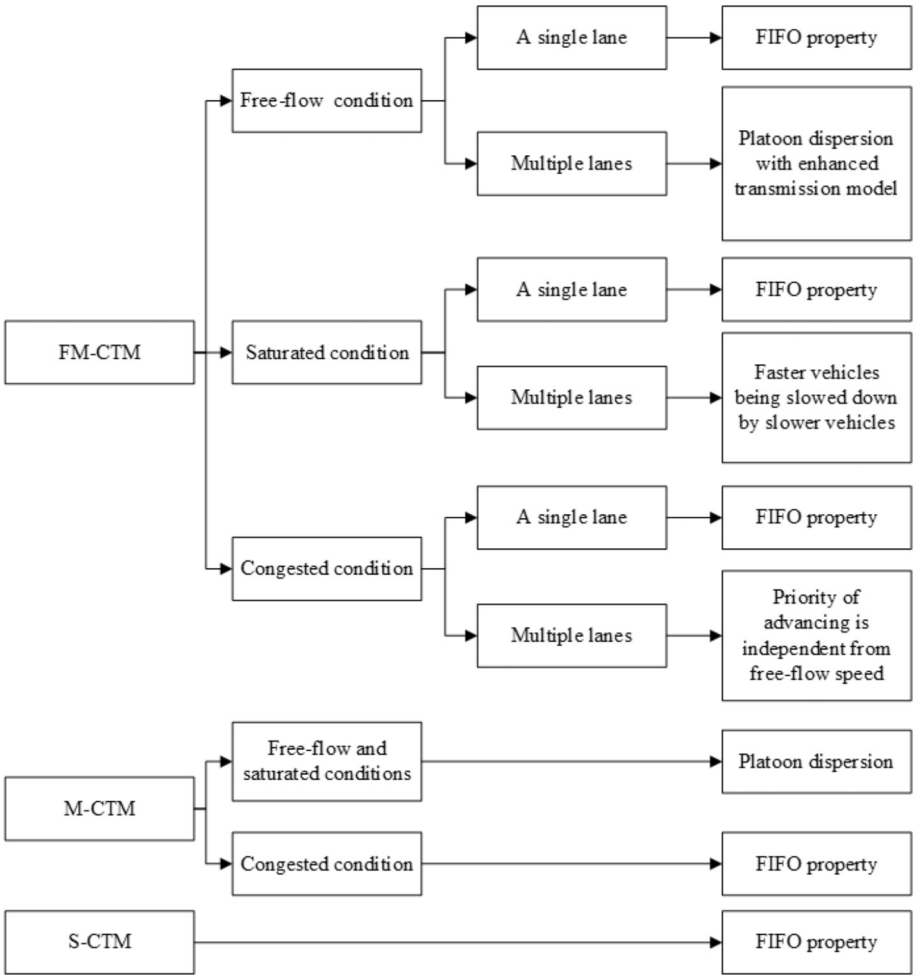

Fig. 2. F-CTM, M-CTM, and S-CTM flow equation formulations.

Table 1
Summary of the different parameters of M-CTM and FM-CTM.

Parameters	M-CTM	FM-CTM
$\Gamma_{i,m}(t)$ for free-flow condition	$\tilde{v}_m$	$\frac{2\tilde{v}_m - 1}{\tilde{v}_m}$
$\Gamma_{i,m}(t)$ for saturated condition	$\tilde{v}_m$	$\frac{2\min(\tilde{v}_m, \bar{v}) - 1}{\min(\tilde{v}_m, \bar{v})}$
$\Gamma_{i,m}(t)$ for congested condition	$\tilde{v}_m$	$\frac{2\tilde{v}_j - 1}{\tilde{v}_j}$
$\frac{\lambda_{i+1,m}}{\sum_{m=1}^{M}\lambda_{i+1,m}}$ for one lane	$\frac{1}{M}, \forall m$	$\frac{1}{M}, \forall m$
$\frac{\lambda_{i+1,m}}{\sum_{m=1}^{M}\lambda_{i+1,m}}$ for multiple lanes	$\frac{1}{M}, \forall m$	Obtained through calibration for each class and link individually
k_i	Unused because $\Gamma_{i,m}(t)$ is always equal to $\tilde{v}_m$	Obtained through calibration for each class and cell individually

The later part of Section 2 is FM-CTM formulation according to Fig. 2 and Table 1. The proposed multiclass traffic models are introduced. For simplification, the flow calculation is organized into two parts: head-of-cell and end-of-cell flow calculations.

2.1. Head-of-cell flow calculation

Head-of-cell vehicle is defined as a vehicle that cannot move forward to the designated cell in the previous time slot so they are assumed to be at the head of cell. As a result, the more congested the traffic is, the more head-of-cell vehicles there

are. Thus, how head-of-cell vehicles move forward to the next cell depends on how each class of vehicles make their advance during congested condition. In the previous work, all head-of-cell vehicles are assumed to have an equal chance to advance to the next cell, regardless of vehicle class or the number of lanes. However, during congestion, a slow vehicle may be more aggressive and overtakes a vehicle class with faster free-flow speed if lane change is allowed (Nair et al., 2011). In case there is only one lane, the FIFO property is enforced. In either case, the priority of advancing to the next cell is independent of the free-flow speed. Thus, the new head-of-cell flow calculation is formulated separately into two cases as follows:

1. The downstream cell has enough remaining space to receive all head-of-cell vehicles from the upstream cell. The mathematical condition for this case is $\sum_{m=1}^{M}[l_m a_{i,m}(t)] < \tilde{r}_{i+1}(t)$. $a_{i,m}$ is the number of head-of-cell vehicles of class m in cell i at time slot t. In this case all head-of-cell vehicles can advance to the downstream cell, and the head-of-cell flow is equal to the number of head-of-cell vehicles in cell i as in Eq. (2)

$$y_{i+1,m,a}(t) = a_{i,m}(t) \tag{2}$$

where $y_{i+1,m,a}(t)$ is the head-of-cell flow on link $i+1$ of class-m at time slot t.

2. The ending cell does not have enough remaining space to receive all head-of-cell vehicles from the beginning cell. The mathematical condition for this case is $\sum_{m=1}^{M}[l_m a_{i,m}(t)] \geqslant \tilde{r}_{i+1}(t)$. In this case, not all head-of-cell vehicles can advance to the downstream cell. Head-of-cell flow of each class is proportional to an overtaking factor of that class, which is defined in Eq. (3)

$$y_{i+1,m,a}(t) = \frac{\lambda_{i+1,m} a_{i,m}(t)\tilde{r}_{i+1}(t)}{\sum_{m=1}^{M}\lambda_{i+1,m} l_m a_{i,m}(t)} \tag{3}$$

where $\lambda_{i+1,m}$ is the overtaking factor of class-m head-of-cell vehicles on link $i+1$. The greater the overtaking factor is, the more priority is placed for class-m head-of-cell to advance to the downstream cell. The overtaking factor is determined by the number of lanes of link $i+1$ and relative overtaking capability of each vehicle class. For a case of a single lane, FIFO property is enforced so that $\frac{\lambda_{i+1,m}}{\sum_{m=1}^{M}\lambda_{i+1,m}} = \frac{1}{M}, \forall m = 1, \ldots, M$. For a multi-lane case, the overtaking factor of each class is expectedly obtained through parameter calibration.

2.2. End-of-cell flow calculation

End-of-cell vehicle is a vehicle that just enters the upstream cell in the previous time slot. Hence, not all end-of-cell vehicles can advance to the downstream cell in one time slot. A proportion of end-of-cell vehicles that are ready to advance the downstream cell in one time slot is determined by the traffic condition and its transmission factor, denoted as $\Gamma_{i,m}(t)$. The transmission factor is a function with respect to the free-flow speed that is calculated based on the traffic condition. In the prior M-CTM, end-of-cell vehicles are assumed to be distributed uniformly in the upstream cell regardless of their free-flow speeds or classes. However, slow vehicles that just enter the upstream cell in the previous time slot should not be able to advance too far in the cell. Hence, in this paper, their distribution along the length of the upstream cell is determined by their normalized free-flow speed $\tilde{v}_m$.

Assuming a free-flow traffic condition, a vehicle with its normalized free-flow speed $\tilde{v}_m$ can travel as far as $h\tilde{v}_m$, where h is the cell length. Thus, their location is between 0 and $h\tilde{v}_m$ distance in the upstream cell. Only vehicles between $h - h\tilde{v}_m$ and h can advance to the downstream cell. Assume the vehicles are uniformly distributed between 0 and $h\tilde{v}_m$, the vehicles that are ready to advance to the downstream cell in the time slot t are proportional to $\frac{h\tilde{v}_m-(h-h\tilde{v}_m)}{h\tilde{v}_m} = \frac{2\tilde{v}_m-1}{\tilde{v}_m}$ as shown in Fig. 3. Therefore, the transmission factor of class-m of cell i at time slot t in free-flow condition is shown in Eq. (4)

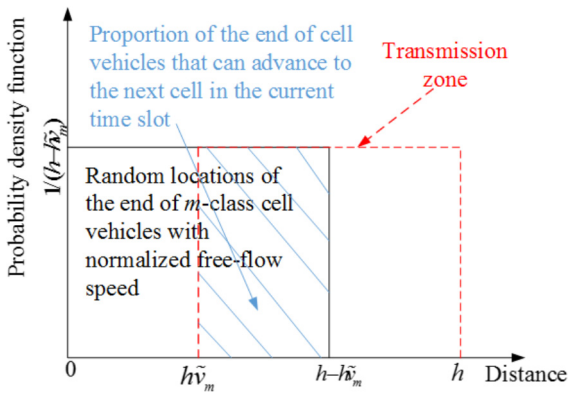

Fig. 3. The proportion of end-of-cell vehicles that is ready to advance to the downstream cell.

$$\Gamma_{i,m}(t) = \frac{2\tilde{v}_m - 1}{\tilde{v}_m} \tag{4}$$

We also define the total sending capability of class-m vehicle of cell i at time slot t as the maximum number of vehicles that can advance to the downstream cell as in Eq. (5)

$$s_{i,m}(t) = a_{i,m}(t) + \left(\frac{2\tilde{v}_m - 1}{\tilde{v}_m}\right) b_{i,m}(t) \tag{5}$$

The calculation for the transmission factor $\Gamma_{i,m}(t)$ can be divided into the following 3 cases:

1. Free-flow condition

We assume the upstream cell is in free-flow condition if the total number of vehicles ready to advance to the downstream cell is no greater than the maximum flow capacity of link $i+1$, $q_{i+1}(t)$. There is no competition to enter the downstream cell if there is enough receiving capability. The condition for this case is $\sum_{m=1}^{M} s_{i,m}(t) \leqslant q_{i+1}(t)$.

As the upstream cell is in free-flow condition, fast vehicles can freely overtake slow vehicles and drive with their free-flow speed without interruption from other classes. Hence, the transmission factor for this condition case is shown in Eq. (6)

$$\Gamma_{i,m}(t) = \frac{2\tilde{v}_m - 1}{\tilde{v}_m}, \quad \forall m = 1, \ldots, M \tag{6}$$

2. Saturated condition

In this case, overtaking can occur, but there is an interruption from other classes. A slow vehicle can partially interrupt a fast vehicle. We assume the upstream cell is in saturated condition if the total number of vehicles ready to advance to the downstream cell is less than the congested density. The condition for this case is $q_{i+1}(t) < \sum_{m=1}^{M} s_{i,m}(t) < k_i c_i$. $k_i c_i$ is the congested density of cell i. k_i is obtained through parameter calibration. Approximately, the lower and upper bounds of k_i are $q_{i+1}(t)/c_i$ and 1. Let $\bar{v}$ be the average free flow speed of the end-of-cell vehicles of cell i being prompt to move to the downstream cell $i+1$

$$\bar{v} = \frac{\sum_{m=1}^{M} \tilde{v}_m s_{i,m}(t)}{\sum_{m=1}^{M} s_{i,m}(t)} \tag{7}$$

A vehicle class faster than the average normalized free-flow speed is slowed down and has to lower their speed. Thus, their transmission factor drops to be the same as that of a vehicle with average free-flow speed as shown in Eq. (8)

$$\Gamma_{i,m}(t) = \frac{2\bar{v} - 1}{\bar{v}}, \quad \text{if} \quad \tilde{v}_m > \bar{v} \tag{8}$$

On the other hand, a vehicle class slower than the average free-flow speed is unaffected by the traffic condition as its free-flow speed is already low. Their transmission factor is shown in Eq. (9)

$$\Gamma_{i,m}(t) = \frac{2\tilde{v}_m - 1}{\tilde{v}_m}, \quad \text{if} \quad \tilde{v}_m \leqslant \bar{v} \tag{9}$$

With Eqs. (8) and (9), the transmission factor for any vehicle classes in saturated condition case is obtained as in Eq. (10)

$$\Gamma_{i,m}(t) = \frac{2\min(\tilde{v}_m, \bar{v}) - 1}{\min(\tilde{v}_m, \bar{v})} \tag{10}$$

3. Congested condition

When the total number of vehicles is greater than the congested density, there is no remaining space in the upstream cell for fast vehicles to overtake slow vehicles. FIFO property is enforced. Then the condition for this case is $\sum_{m=1}^{M} s_{i,m}(t) \geqslant c_i k_i$. Let j be the slowest vehicle class that is in cell i at time slot t. Then all vehicle classes advance at the same speed as the class j. Hence, the transmission factor in this case is obtained as in Eq. (11)

$$\Gamma_{i,m}(t) = \frac{2\tilde{v}_j - 1}{\tilde{v}_j}, \quad \forall m = 1, \ldots, M \tag{11}$$

Note that, for a single lane, k_i may be a very small number, indicating that FIFO occurs at much lower density than a case of multiple lanes. In other word, saturated condition is very narrowly ranged.

The example of transmission factors for the three traffic conditions is shown in Fig. 4 where the three colored lines represent three vehicle classes with normalized free-flow speeds of 1, 0.75 and 0.5. In free-flow condition, the transmission factors are calculated based on their free-flow speeds. In saturated condition, assuming an average normalized free-flow speed = 0.66, the transmission factors of two vehicle classes with normalized free-flow speed greater than 0.66 deceases to 0.66 as these two faster vehicle classes cannot overtake slower vehicle class comfortably. In congested condition, FIFO property is enforced. Hence, the transmission factors of all three vehicle classes decease to that of the slowest vehicle class.

After the transmission factors are calculated, the flow of end-of-cell vehicles can be obtained. After head-of-cell vehicles enter the downstream cell, end-of-cell vehicles can advance to the downstream cell if there is remaining receiving capability. Hence, we define the relative receiving capability after receiving head-of-cell vehicles of cell $i+1$ at time slot t, $\tilde{r}^*_{i+1}(t)$, as in Eq. (12)

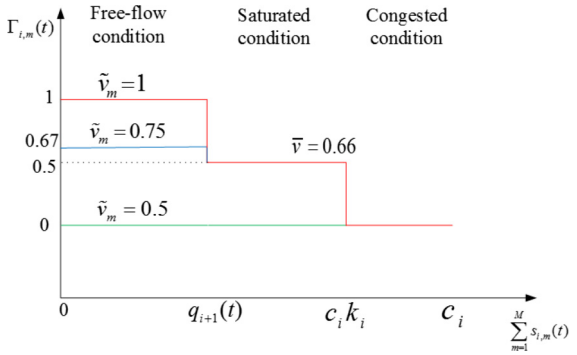

Fig. 4. Transmission factors of three vehicle classes in three traffic conditions.

$$\tilde{r}^*_{i+1}(t) = \tilde{r}_{i+1} - \sum_{m=1}^{M}[l_m a_{i,m}(t)] \tag{12}$$

Flow calculation of end-of-cell can be divided according to $\tilde{r}^*_{i+1}(t)$ into the following 2 cases:

1. The downstream cell cannot receive all head-of-cell vehicles The condition for this case is $\tilde{r}^*_{i+1}(t) < 0$. There is no space for end-of-cell vehicles. Thus, the end-of- cell flow is zero:

$$y_{i+1,m,b}(t) = 0, \quad \forall m \tag{13}$$

where $y_{i+1,m,b}(t)$ is the end-of-cell flow of class-m on link $i+1$.

2. The downstream cell can receive all head-of-cell vehicles

The condition for this case is $\tilde{r}^*_{i+1}(t) \geqslant 0$. In this case, there is still a remaining space for end-of-cell vehicles to enter the downstream cell. This case can be further divided into 2 subcases

2.1. The downstream cell can receive all end-of-cell vehicles

The condition for this subcase is $\tilde{r}^*_{i+1}(t) \geqslant \Gamma_{i,m}(t)b_{i,m}(t)$. In this case, all prompt end-of-cell vehicles can advance to cell $i+1$ as in Eq. (14)

$$y_{i+1,m,b}(t) = \Gamma_{i,m}(t)b_{i,m}(t) \tag{14}$$

2.2. The downstream cell cannot receive all end-of-cell vehicles. The condition for this subcase is $\tilde{r}^*_{i+1}(t) < \Gamma_{i,m}(t)b_{i,m}(t)$. Only a portion of end-of-cell vehicles can advance to the downstream cell.

$$y_{i+1,m,b}(t) = \frac{\Gamma_{i,m}(t)b_{i,m}(t)\tilde{r}^*_{i+1}(t)}{\sum_{m=1}^{M}[\Gamma_{i,m}(t)l_m b_{i,m}(t)]} \tag{15}$$

where $\sum_{m=1}^{M}\tilde{l}_m y_{i+1,m,b}(t) = \tilde{r}^*_{i+1}(t)$ the total flow $y_{i+1,m}(t)$ of vehicle class-m is the sum of head-of-cell and end-of-cell vehicle class-m as in Eq. (16)

$$y_{i+1,m}(t) = y_{i+1,m,a}(t) + y_{i+1,m,b}(t) \tag{16}$$

The flow equations from Eqs. (1)–(16) can be reduced to the closed-form equation in Eq. (17)

$$\begin{aligned} y_{i+1,m}(t) = \min &\left\{a_{i,m}(t), \frac{\lambda_{i+1,m}a_{i,m}(t)\tilde{r}_{i+1}(t)}{\sum_{m=1}^{M}[\lambda_{i+1,m}l_m a_{i,m}(t)]}\right\} + \\ &\text{median}\left\{0, \frac{\Gamma_{i,m}(t)b_{i,m}(t)\tilde{r}^*_{i+1}(t)}{\sum_{m=1}^{M}[\Gamma_{i,m}(t)l_m b_{i,m}(t)]}, \Gamma_{i,m}(t)b_{i,m}(t)\right\} \end{aligned} \tag{17}$$

Eq. (17) is rewritten to closed-form matrix equations as in Eqs. (18)–(20)

$$\vec{Y}_{i+1,a}(t) = \min\left\{\vec{A}_i(t), \frac{\tilde{r}_{i+1}(t)}{\overrightarrow{\lambda_{i+1}}^T diag(\vec{\tilde{L}})\vec{A}_i(t)} diag(\overrightarrow{\lambda_{i+1}})\vec{A}_i(t)\right\} \tag{18}$$

$$\vec{Y}_{i+1,b}(t) = \text{median}\left\{\vec{0}_{M\times 1}, \frac{\tilde{r}^*_{i+1}(t)}{\vec{\Gamma}_i^T(t)diag(\vec{\tilde{L}})\vec{B}_i(t)} diag(\vec{\Gamma}_i(t))\vec{B}_i(t), diag(\vec{\Gamma}_i(t))\vec{B}_i(t)\right\} \tag{19}$$

$$\vec{Y}_{i+1}(t) = \vec{Y}_{i+1,a}(t) + \vec{Y}_{i+1,b}(t) \tag{20}$$

with

$$\Gamma_{i,m}(t)=\begin{cases}\frac{2\tilde{v}_m-1}{\tilde{v}_m} & ,\sum_{m=1}^{M}s_{i,m}(t)\leqslant q_{i+1}(t)\\ \frac{2\min(\tilde{v}_m,\tilde{v})-1}{\min(\tilde{v}_m,\tilde{v})} & ,q_{i+1}(t)<\sum_{m=1}^{M}s_{i,m}(t)<k_ic_i\\ \frac{2\tilde{v}_j-1}{\tilde{v}_j} & ,\sum_{m=1}^{M}s_{i,m}(t)\geqslant k_ic_i\end{cases}$$

where $\vec{A}_i(t)=[a_{i,1}(t),\ldots,a_{i,M}(t)]^T$, $\vec{B}_i(t)=[b_{i,1}(t),\ldots,b_{i,M}(t)]^T$, $\vec{N}_{i+1}(t)=[n_{i+1,1}(t),\ldots,n_{i+1,M}(t)]^T$, $\vec{Y}_{i+1,a}(t)=[y_{i+1,1,a}(t),\ldots,y_{i+1,M,a}(t)]^T$, $\vec{Y}_{i+1,b}(t)=[y_{i+1,1,b}(t),\ldots,y_{i+1,M,b}(t)]^T$, $\vec{Y}_{i+1}(t)=[y_{i,1}(t),\ldots,y_{i,M}(t)]^T$, $\vec{\tilde{L}}=[\tilde{l}_1,\ldots,\tilde{l}_M]^T$, $\overrightarrow{\lambda_{i+1}}=[\lambda_{i+1,1},\ldots,\lambda_{i+1,M}]^T$, $\vec{\Gamma}_i(t)=[\Gamma_{i,1}(t),\ldots,\Gamma_{i,M}(t)]^T$, $diag(\overrightarrow{\lambda_{i+1}})=\begin{bmatrix}\lambda_{i+1,1}&0&\cdots&0\\0&\lambda_{i+1,2}&\cdots&0\\\vdots&\vdots&\ddots&\vdots\\0&0&\cdots&\lambda_{i+1,M}\end{bmatrix}$, $diag(\vec{\Gamma}_i(t))=\begin{bmatrix}\Gamma_{i,1}(t)&0&\cdots&0\\0&\Gamma_{i,2}(t)&\cdots&0\\\vdots&\vdots&\ddots&\vdots\\0&0&\cdots&\Gamma_{i,M}(t)\end{bmatrix}$, $diag(\vec{\tilde{L}})=\begin{bmatrix}\tilde{l}_1&0&\cdots&0\\0&\tilde{l}_2&\cdots&0\\\vdots&\vdots&\ddots&\vdots\\0&0&\cdots&\tilde{l}_M\end{bmatrix}$.

Finally, the flows of every vehicle class from the upstream cell to the downstream cell are obtained from Eqs. (18)–(20). The detail of the formulation of the closed-form equation is elaborated in the Appendix A section.

After the flows are obtained through Eqs. (18)–(20), the number of vehicles in each cell can be updated by the flow conservation law as follows:

$$\vec{A}_i(t+1)=\vec{N}_i(t)-\vec{Y}_{i+1}(t) \tag{21}$$

$$\vec{B}_i(t+1)=\vec{Y}_i(t) \tag{22}$$

$$\vec{N}_i(t+1)=\vec{A}_i(t+1)+\vec{B}_i(t+1) \tag{23}$$

Note that, by substituting $\vec{A}_i(t+1)$ and $\vec{B}_i(t+1)$ in Eq. (23) with Eqs. (21) and (22), the flow conservation law of S-CTM is obtained.

Please note that the closed-form formulation in Appendix A section can be applied to M-CTM as well. By substituting $\Gamma_{i,m}(t)$ and $\lambda_{i+1,m}$ with values from Table 1, the closed-form M-CTM is obtained in Eqs. (24)–(26). Hence, FM-CTM is a general form of M-CTM and, by extension, S-CTM.

$$\vec{Y}_{E,a}(t)=\min\left\{\vec{A}_{Bg}(t),\frac{\tilde{r}_E(t)}{\vec{\tilde{V}}^T diag(\vec{\tilde{L}})\vec{A}_{Bg}(t)}diag(\vec{\tilde{V}})\vec{A}_{Bg}(t)\right\} \tag{24}$$

$$\vec{Y}_{E,b}(t)=\mathrm{mid}\left\{\vec{0}_{M\times 1},\frac{\tilde{r}^*_E(t)}{\vec{\tilde{V}}^T diag(\vec{\tilde{L}})\vec{B}_{Bg}(t)}diag(\vec{\tilde{V}})\vec{B}_{Bg}(t),diag(\vec{\tilde{V}})\vec{B}_{Bg}(t)\right\} \tag{25}$$

$$\vec{Y}_E(t)=\vec{Y}_{E,a}(t)+\vec{Y}_{E,b}(t) \tag{26}$$

3. Convergence to the single class LWR model

S-CTM is one of discrete solutions of LWR model, hence S-CTM converges to LWR model when the cell length approaches zero. Hence, in order to prove that FM-CTM can converge to LWR, one needs to prove that FM-CTM converges to S-CTM. Let every vehicle class be identical by setting all their parameters to be the same. If the total calculated vehicle-class flows from FM-CTM is equal to the total calculated flow from S-CTM, then FM-CTM converges to S-CTM.

Let vehicle class $m = 1, \ldots, M$ be identical then we obtain $l_m = l_1, \tilde{l}_m = 1, \vec{\tilde{L}} = \vec{1}_{M\times 1}, diag(\vec{\tilde{L}}) = I_{M\times M}, \psi_{i+1,m} = 1, \lambda_{i+1,m} = \lambda_{i+1,1}$, $\overrightarrow{\lambda_{i+1}} = \lambda_{i+1,1}\vec{1}_{M\times 1}$, $diag(\overrightarrow{\lambda_{i+1}}) = \lambda_{i+1,1} I_{M\times M}$, $\tilde{v}_m = 1, \bar{v} = 1, \Gamma_{i,m}(t) = 1, \vec{\Gamma}_i(t) = \vec{1}_{M\times 1}$.

Substitute the above parameters to Eq. (1), we obtain $\tilde{r}_{i+1}(t) = \min\{q_{i+1}(t), \delta_{i+1}(c_{i+1} - \sum_{m=1}^{M}(n_{i+1,m}(t)))\}$. Let $\sum_{m=1}^{M}(n_{i+1,m}(t)) = n_{i+1}(t)$ then

$$\tilde{r}_{i+1}(t) = \min\{q_{i+1}(t), \delta_{i+1}(c_{i+1} - n_{i+1}(t))\} = r_{i+1}(t) \tag{27}$$

where $r_{i+1}(t)$ is receiving capability of S-CTM. Likewise, Eq. (12) is reduced to Eq. (28)

$$\tilde{r}^{*}_{i+1}(t) = r_{i+1}(t) - \sum_{m=1}^{M} a_{i,m}(t) \tag{28}$$

Then Eq. (18) is reduced to Eq. (29)

$$\begin{aligned}\vec{Y}_{i+1,a}(t) &= \min\left\{\vec{A}_i(t), \frac{r_{i+1}(t)}{\vec{1}_{1\times M} I_{M\times M}\vec{A}_i(t)}\lambda_{i+1,1} I_{M\times M}\vec{A}_i(t)\right\} \\ &= \min\left\{\vec{A}_i(t), \frac{r_{i+1}(t)}{\sum_{i=1}^{M}\lambda_{i+1,1}a_i}\lambda_{i+1,1}\vec{A}_i(t)\right\} = \min\left\{\vec{A}_i(t), \frac{r_{i+1}(t)\vec{A}_i(t)}{\sum_{i=1}^{M}a_i}\right\}\end{aligned} \tag{29}$$

Total head-of-cell flow is obtained by summation of head-of-cell flows of Eq. (29) as in Eq. (30),

$$\sum_{i=1}^{M} y_{i+1,m,a}(t) = \min\left\{\sum_{m=1}^{M} a_i(t), \frac{r_{i+1}(t)\sum_{m=1}^{M} a_i(t)}{\sum_{i=1}^{M} a_i}\right\} = \min\left\{\sum_{m=1}^{M} a_i(t), r_{i+1}(t)\right\} \tag{30}$$

Then Eq. (19) is reduced to Eq. (31)

$$\begin{aligned}\vec{Y}_{i+1,b}(t) &= \text{median}\left\{\vec{0}_{M\times 1}, \frac{r_{i+1}(t) - \sum_{m=1}^{M} a_{i,m}(t)}{\vec{1}_{1\times M} I_{M\times M}\vec{B}_i(t)} I_{M\times M}\vec{B}_i(t), I_{M\times M}\vec{B}_i(t)\right\} \\ &= \text{median}\left\{\vec{0}_{M\times 1}, \frac{r_{i+1}(t) - \sum_{m=1}^{M} a_{i,m}(t)}{\sum_{m=1}^{M} b_i(t)}\vec{B}_i(t), \vec{B}_i(t)\right\}\end{aligned} \tag{31}$$

Total end-of-cell flow is obtained by summation of end-of-cell flows of Eq. (31) as in Eq. (32)

$$\begin{aligned}\sum_{m=1}^{M} y_{i+1,m,b}(t) &= \text{median}\left\{0, \frac{r_{i+1}(t) - \sum_{m=1}^{M} a_{i,m}(t)}{\sum_{m=1}^{M} b_i(t)}\sum_{m=1}^{M} b_i(t), \sum_{m=1}^{M} b_i(t)\right\} \\ &= \text{median}\left\{0, r_{i+1}(t) - \sum_{m=1}^{M} a_{i,m}(t), \sum_{m=1}^{M} b_i(t)\right\}\end{aligned} \tag{32}$$

From Eqs. (30) and (32), we obtain total flow as follow:

$$\sum_{m=1}^{M}(y_{i+1,m,a}(t) + y_{i+1,m,b}(t)) = \min\left\{\sum_{m=1}^{M} a_i(t), r_{i+1}(t)\right\} + \text{median}\left\{0, r_{i+1}(t) - \sum_{m=1}^{M} a_{i,m}(t), \sum_{m=1}^{M} b_i(t)\right\} \tag{33}$$

To compute Eq. (33), one may divide the condition into 3 cases,

1. Total sum of head-of-cell and end-of-cell vehicles is less than the receiving capability. The mathematic condition for this case is $\sum_{m=1}^{M} a_i(t) + \sum_{m=1}^{M} b_i(t) \leqslant r_{i+1}(t)$. As a result, $\sum_{m=1}^{M} a_i(t) \leqslant r_{i+1}(t)$ and $\sum_{m=1}^{M} b_i(t) \leqslant r_{i+1}(t)$. The solution of Eq. (33) in this case is $\sum_{m=1}^{M}(y_{i+1,m,a}(t) + y_{i+1,m,b}(t)) = \sum_{m=1}^{M} a_i(t) + \sum_{m=1}^{M} b_i(t)$ if $\sum_{m=1}^{M} a_i(t) + \sum_{m=1}^{M} b_i(t) \leqslant r_{i+1}(t)$. From Eq. (23), $\sum_{m=1}^{M} a_i(t) + \sum_{m=1}^{M} b_i(t) = \sum_{m=1}^{M} n_{i,m}(t) = n_i(t)$ where $n_i(t)$ is also the number of vehicles in S-CTM. Then Eq. (34) is obtained from Eq. (33)

$$\sum_{m=1}^{M}(y_{i+1,m,a}(t) + y_{i+1,m,b}(t)) = n_i(t) \text{ if } n_i(t) \leqslant r_{i+1}(t) \tag{34}$$

2. Total head-of-cell vehicles are greater than the receiving capability. The mathematic condition is $\sum_{m=1}^{M} a_i(t) > r_{i+1}(t)$. The condition implies $n_i(t) > r_{i+1}(t)$ and $r_{i+1}(t) - \sum_{m=1}^{M} a_i(t) < 0 < \sum_{m=1}^{M} b_i(t)$. Thus, the solution of Eq. (33) in this case is obtained as in Eq. (35)

$$\sum_{m=1}^{M}\left(y_{i+1,m,a}(t)+y_{i+1,m,b}(t)\right)=r_{i+1}(t)+0=r_{i+1}(t)\ \text{ if } n_i(t)>r_{i+1}(t) \tag{35}$$

3. Total head-of-cell vehicles are less than the receiving capability, but total sum of head-of-cell and end-of-cell vehicles is not. The mathematic condition for this case is $\sum_{m=1}^{M}a_i(t)\leqslant r_{i+1}(t)$ and $\sum_{m=1}^{M}a_i(t)+\sum_{m=1}^{M}b_i(t)>r_{i+1}(t)$. The condition implies $\sum_{m=1}^{M}b_i(t)>r_{i+1}(t)-\sum_{m=1}^{M}a_i(t)>0$. Thus, the solution of Eq. (33) in this case is obtained as in Eq. (36)

$$\sum_{m=1}^{M}\left(y_{i+1,m,a}(t)+y_{i+1,m,b}(t)\right)=\sum_{m=1}^{M}a_i(t)+r_{i+1}(t)-\sum_{m=1}^{M}a_{i,m}(t)=r_{i+1}(t)\ \text{ if } n_i(t)>r_{i+1}(t) \tag{36}$$

From the three solutions of Eq. (33) from Eqs. (34)–(36), we obtain the total flow of FM-CTM as in Eq. (37)

$$\begin{aligned}\sum_{m=1}^{M}(y_{i+1,m,a}(t)+y_{i+1,m,b}(t))&=\begin{cases}n_i(t), n_i(t)\leqslant r_{i+1}(t)\\ r_{i+1}(t), n_i(t)>r_{i+1}(t)\\ r_{i+1}(t), n_i(t)>r_{i+1}(t)\end{cases}\\ &=\min(n_i(t),r_{i+1}(t))\end{aligned} \tag{37}$$

Since $y_{i+1}(t)=\min(n_i(t),r_{i+1}(t))$ where $y_{i+1}(t)$ is the total flow from S-CTM's flow equation, then $\sum_{m=1}^{M}(y_{i+1,m,a}(t)+y_{i+1,m,b}(t))=y_{i+1}(t)$. The total flow of FM-CTM is equal to the total flow of S-CTM when every vehicle class is identical. Therefore, FM-CTM can converge to S-CTM and, by extension, LWR model.

4. Numerical results

This section of numerical results is intended to study the cases where

1. FM-CTM outperforms M-CTM in the free-flow condition with the new transmission function, and
2. the proposed M-CTM is significantly more accurate than the prior M-CTM when there are both platoon dispersion and FIFO behaviors on the road network, and
3. FM-CTM is validated with real-world data.

There are 3 cases of experiments:

Case 1: Non-stationary vehicle composition
Case 2: FIFO and lane-varying network
Case 3: Evaluation based on real data from freeway I-80

The network topologies of cases 1, 2, and 3 are shown in Figs. 5–7. Cells S1 and S2 are boundary entry cells to input a boundary entry flow from either VISSIM or real-world data. S3 is a boundary exit cell. For cases 1 and 2, there is no restriction on the incoming flow to S3. On the other hand, there is congestion propagating back from downstream in case 3, the boundary flow to cell S3 is therefore set to the boundary flow exit, obtained from the real-world data.

4.1. Parameter calibration

To avoid a bias from training data when comparing between CTMs, we use the same data set as training and evaluation data. In cases 1 and 2, microscopic simulation, VISSIM (Vissim, 2008) is adopted as the ground truth. In case 3, the real-world data is used to validate the proposed FM-CTM. The simulated densities from both proposed FM-CTM and M-CTM from (Tuerprasert and Aswakul, 2010) are compared with the observed density from VISSIM or from the real-world data to compute the root-mean-square errors (RMSE) as shown in Eqs. (38)–(40).

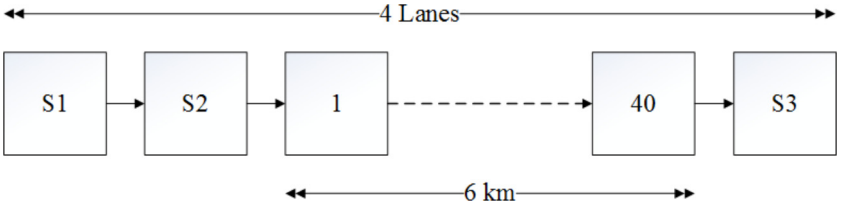

Fig. 5. Assumed network topology of case 1.

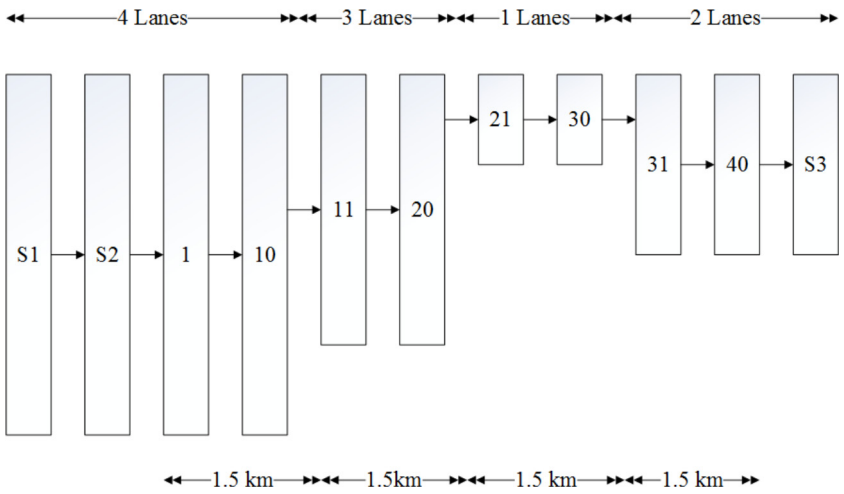

Fig. 6. Assumed network topology for case 2.

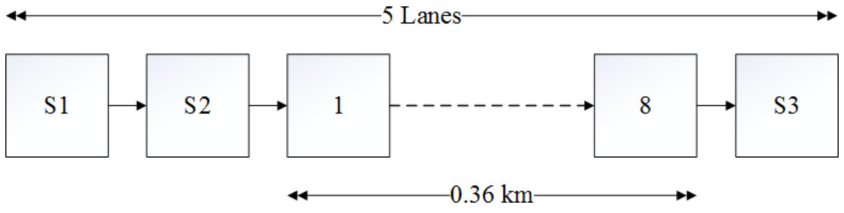

Fig. 7. Real network topology of case 3.

$$RMSE_{PV} = \sqrt{\frac{\sum_{i=1}^{I}\sum_{t=1}^{T}\left(\hat{n}_{i,PV}(t) - n_{i,PV}(t)\right)^2}{T \cdot I}} \tag{38}$$

$$RMSE_{HV} = \sqrt{\frac{\sum_{i=1}^{I}\sum_{t=1}^{T}\left(\hat{n}_{i,HV}(t) - n_{i,HV}(t)\right)^2}{T \cdot I}} \tag{39}$$

$$RMSE_{total} = RMSE_{PV} + RMSE_{HV} \tag{40}$$

where $\hat{n}_{i,PV}(t)$ and $\hat{n}_{i,HV}(t)$ are observed densities of PVs and HVs from either VISSIM or the real-world data and $n_{i,PV}(t)$ and $n_{i,HV}(t)$ are the simulated densities of PVs and HVs from either FM-CTM or M-CTM. The $RMSE_{total}$, defined as the summation of RMSEs of a class, is to evaluate density estimation for each class individually. I and T are the total number of observed cells and time slots, varying from case to case.

$RMSE_{total}$ in Eq. (40) is also used as a fitness function to calibrate both FM-CTM and M-CTM to obtain the unknown calibrated parameters. The calibrated parameters are obtained through the fitness function, which can be minimized using

Table 2
Resultant FM-CTM and M-CTM calibrated parameters for cases 1 and 2.

Calibration parameters	Lower bounds	Upper bounds	FM-CTM Case 1	FM-CTM Case 2	M-CTM Case 1	M-CTM Case 2
q_{4lanes} (per lane per sec)	0.37	0.7877	0.49	0.45	0.49	0.37
q_{3lanes} (per lane per sec)	0.37	0.7877	–	0.38	–	0.45
q_{2lanes} (per lane per sec)	0.37	0.7877	–	0.46	–	0.38
q_{1lane} (per lane per sec)	0.37	0.7877	–	0.66	–	0.69
l_{PV} (m)	4	6	6	5.45	5.36	4.74
l_{HV} (m)	11	13	11.21	12.98	12.46	12.74
∂_i	0.3	1	0.39	0.31	0.58	0.32

genetic algorithm (GA). The calibrated parameters are set as the population vector of GA. The generation and population numbers are set to 100 and 20. The other GA settings are the same as the default settings by Matlab R2012a.

The resultant calibrated final values, lower and upper bounds of all parameters for FM-CTM and M-CTM are shown in Tables 2 and 3, q_{+1}, $\lambda_{i+1,PV}$ and k_i are calibrated based on the number of lanes. $k_{1lane},\ldots,k_{4lane}$ are congested densities for 1-lane to 4-lane cells, respectively. $\lambda_{link11,PV}$, $\lambda_{link21,PV}$, and $\lambda_{link31,PV}$ are the overtaking factors for the bottleneck links between cells 10 and 11, 20 and 21, and 30 and 31, which are calibrated separately from $\lambda_{1lanes,PV},\ldots,\lambda_{4lanes,PV}$ in order to specifically capture the dynamics at the bottlenecks. All overtaking factors of HV, $\lambda_{i+1,HV}$, are equal to $1-\lambda_{i+1,PV}$.

For case 3, to capture the dynamic of the actual traffic in more detail, q_{i+1}, $\lambda_{i+1,PV}$ and k_i are calibrated for the links and cells individually. The resultant q_{i+1} of links 1–8 are shown in Table 4, the resultant $\lambda_{i+1,PV}$ of links 1–8 are 0.20, 0.73, 0.58, 0.66, 0.66, 0.70, 0.76, and 0.77. The resultant k_i of cells 1–8 are 0.63, 0.77, 0.56, 0.57, 0.77, 0.88, 0.14, and 0.93.

Then the resultant calibrated parameters are used to simulate FM-CTM and M-CTM to obtain density estimation results. The resultant $RMSE_{PV}$, $RMSE_{HV}$, $RMSE_{total}$, and comparisons of FM-CTM and M-CTM are shown in Table 5.

4.2. Cases 1&2: Non-stationary vehicle composition&FIFO and lane-varying network

For cases 1 and 2, the selected network is an assumed 6 km-long straight roadway. There are two classes of vehicles, PVs and HVs. The free-flow speeds of PVs and HVs are 108 and 72 km/h, so the normalized free-flow speeds are 1 and 0.66 for PV and HV classes. The vehicle lengths of PVs and HVs are 5 and 12 meters. The lengths plus bumpers of both classes are obtained through parameter calibration. Time interval is 5 s. Hence, the road is divided equally into a series of 40 cascading cells with 150 meters in length. Total simulation time is 3600 s or 720 time slots. The traffic volume and number of lanes vary by individual cases.

Case 1 is designed to verify the new transmission function. Hence, the traffic condition is in free-flow condition for all simulation time. Each cell has 4 lanes and a cell length of 150 meters as shown in Fig. 5. A total of 2000 vehicles enter the network in time-varying rates. The vehicle entries for each class are periodic; however, their entry times are overlapped with each other. PVs enter the network at 0–900 and 1800–2700 s at 3200 vph. HVs enter the network at 750–1050 s and 2700–3000 s at 2400 vph. The boundary input traffic flow of this case is shown in Fig. 8.

The network in case 2 is the same as the network in case 1 but the number of lanes is varied from 1 to 4 as shown in Fig. 6. Cells 1–10, 11–20, 21–30, and 31–40 have 4, 3, 1, and 2 lanes, respectively. The vehicle composition is time constant, 80:20 for PVs:HVs. The total traffic volume is 2000 vph: 1600 and 400 vph for PVs and HVs. The boundary input traffic flow of this case is shown in Fig. 9. This case is designed to observe a bottleneck between cells 20 and 21 and various traffic conditions along the road network. The 1-lane road from cell 21–30 is aimed to verify FIFO property of FM-CTM. The bottleneck due to physical lane drop between cells 20 and 21 is to verify the contribution of overtaking factor $\lambda_{i+1,m}$ to the performance of density estimation. Note that, even though the number of lanes drops from 4 to 3 in cells 10–11, the queue is not observed due to traffic volume being much lower than the saturation rate of 3-lanes road.

As expected, FM-CTM shows improvement over M-CTM and can reduce $RMSE_{total}$ by 9% and 15% in cases 1 and 2. For case 1, FM-CTM and M-CTM have almost the same $RMSE_{PV}$ because this experimental case is designed to test the new transmission function. The fastest-class vehicles are unaffected by the new transmission function because they can always advance to the next cell in a free-flow condition. On the other hand, FM-CTM shows about 18% improvement in $RMSE_{HV}$. This implies the new transmission function estimates HVs' density and, in turn, their transmission even better than M-CTM that is already accurate. The densities estimated by FM-CTM and M-CTM of cell 30, 4.5 km from the upstream, are shown in Figs. 10 and 11.

From time slots 580–720, which is HV only, M-CTM and FM-CTM estimate HVs differently due to different transmission functions. M-CTM tends to estimate the arrival of HVs earlier than the observed data. On the other hand, despite being overall more accurate, HVs' arrival estimated by FM-CTM is lagged behind the observed data. Even though FM-CTM improves the accuracy over M-CTM, FM-CTM still shows substantial modeling error when estimating the density for a long distance from

Table 3
Resultant FM-CTM calibrated parameters for cases 1 and 2.

Calibration parameters	Lower bounds	Upper bounds	FM-CTM case 1	FM-CTM case 2
$\lambda_{4lanes,PV}$	0	1	0.26	0.90
$\lambda_{3lanes,PV}$	0	1	–	0.73
$\lambda_{2lanes,PV}$	0	1	–	0.59
$\lambda_{link11,PV}$	0	1	–	0.67
$\lambda_{link21,PV}$	0	1	–	0.79
$\lambda_{link31,PV}$	0	1	–	0.62
k_{4lane}	0.06	1	0.29	0.31
k_{3lane}	0.06	1	–	0.64
k_{2lane}	0.06	1	–	0.56
k_{1lane}	0.06	1	–	0.13

Table 4
Resultant calibrated parameters for cases 3.

Calibration parameters	Lower bounds	Upper bounds	FM-CTM	M-CTM
q_1 (per lane per sec)	0.37	0.7877	0.70	0.41
q_2	0.37	0.7877	0.47	0.46
q_3	0.37	0.7877	0.49	0.41
q_4	0.37	0.7877	0.62	0.42
q_5	0.37	0.7877	0.57	0.46
q_6	0.37	0.7877	0.43	0.42
q_7	0.37	0.7877	0.45	0.48
q_8	0.37	0.7877	0.42	0.46
l_{PV} (m)	4.26	7.3	7.3	7.2
l_{HV} (m)	14	17	14.5	15.3
∂_i	0.3	1	0.34	0.3

Table 5
Resultant RMSEs of FM-CTM and M-CTM after parameter calibration.

Case	FM-CTM $RMSE_{PV}$	FM-CTM $RMSE_{HV}$	FM-CTM $RMSE_{total}$	M-CTM$RMSE_{PV}$	M-CTM$RMSE_{SV}$	M-CTM $RMSE_{total}$	$RMSE_{total}$ reduction
1	1.08	0.80	1.88	1.09	0.98	2.07	9.2%
2	2.24	1.11	3.35	2.83	1.13	3.96	15.4%
3	2.92	0.80	3.72	3.62	0.80	4.42	15.8%

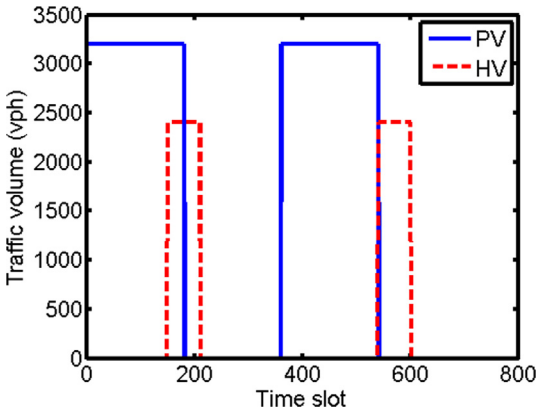

Fig. 8. Boundary input traffic flow for case 1.

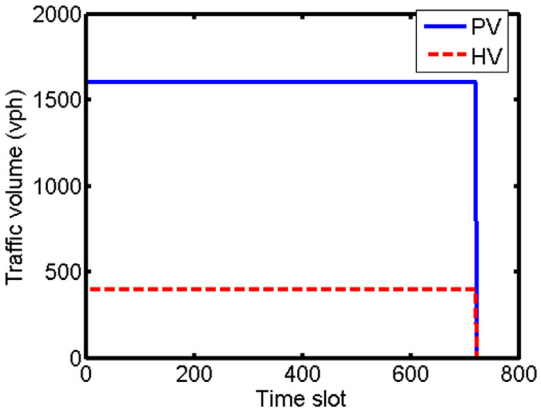

Fig. 9. Boundary input traffic flow for case 2.

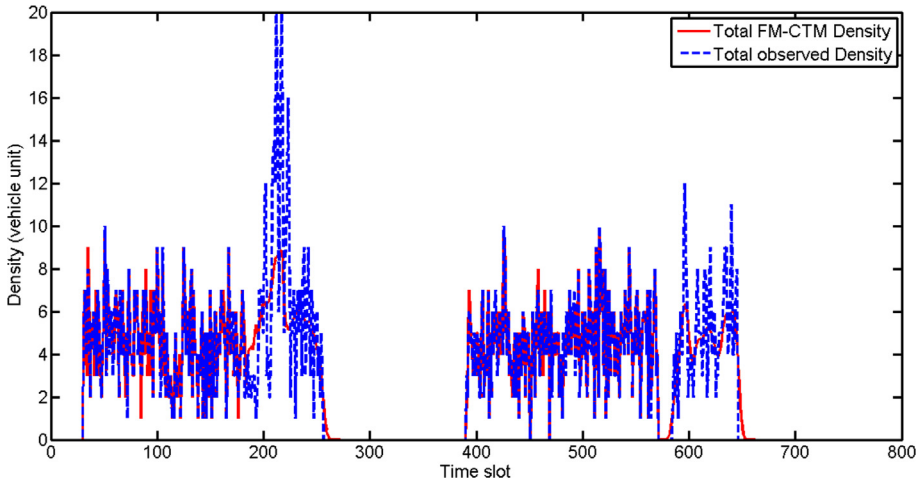

Fig. 10. Case 1: The total FM-CTM density history of cell 30.

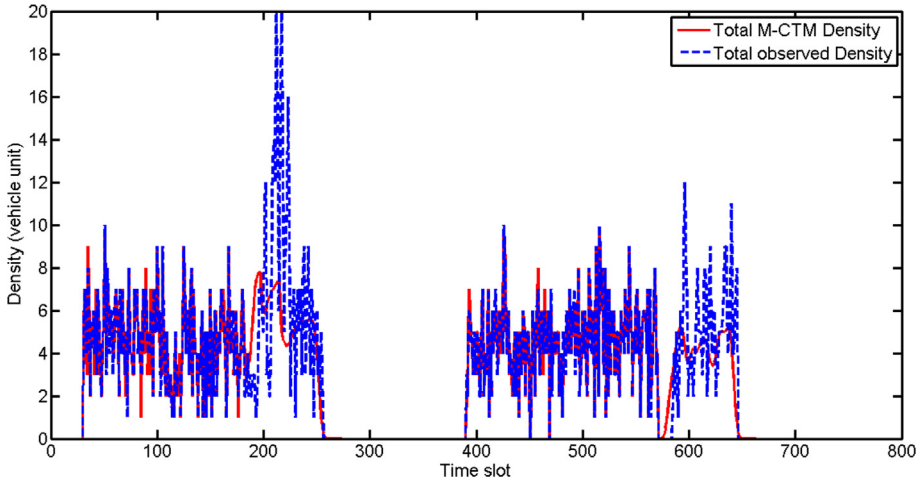

Fig. 11. Case 1: The total M-CTM density history of cell 30.

the boundary entry cells (cells S1 and S2). As a result, FM-CTM' estimation is still benefited from traffic input data with more spatial resolution, e.g. the adjacent loop detectors with moderate distance apart.

For case 1 where $\lambda_{4lanes,PV} = 0.26$, it is a free-flow condition in which the flow calculation is unaffected by the overtaking factor in congested condition, $\lambda_{4lanes,PV}$, hence GA can freely choose any final value of $\lambda_{4lanes,PV}$ without compromising on the fitness function or RMSE value. This is verified further by resimulating FM-CTM in case 1 with $\lambda_{4lanes,PV} > 0.5$. FM-CTM in case 1 still yields the same results as in Table 5 and Fig. 10, regardless of value of $\lambda_{4lanes,PV}$.

For case 2, FM-CTM shows more improvements over M-CTM due to the newly included transmission function and overtaking factor. As expected, k_{1lane} is the lowest among all k_i value in case 2. The reason is FIFO is enforced for a single-lane segment for most traffic condition range. Therefore, GA chooses a small value for k_i in order to enforce FIFO at a lower density. This implies k_i can capture the FIFO property enforced by a single lane very well, allowing FM-CTM to estimate traffic state more accurate than M-CTM.

Cell 20 is the boundary cell where the bottleneck occurs when the number of lanes drops from 3 to 1.

As shown in Figs. 12–14. M-CTM fails to mimic the priority of PVs and HVs to move through the bottleneck link between cells 20 and 21. On the other hand, FM-CTM performs better due to the overtaking factor $\lambda_{link21,PV}$. All the resultants λ_{PV} in case 2 are greater than λ_{HV} because PVs are faster and smaller. Hence, PV outmanoeuvres HV when traffic congestion occurs. The test case which verifies FM-CTM when there is a slower but nimbler vehicle is an interesting future work.

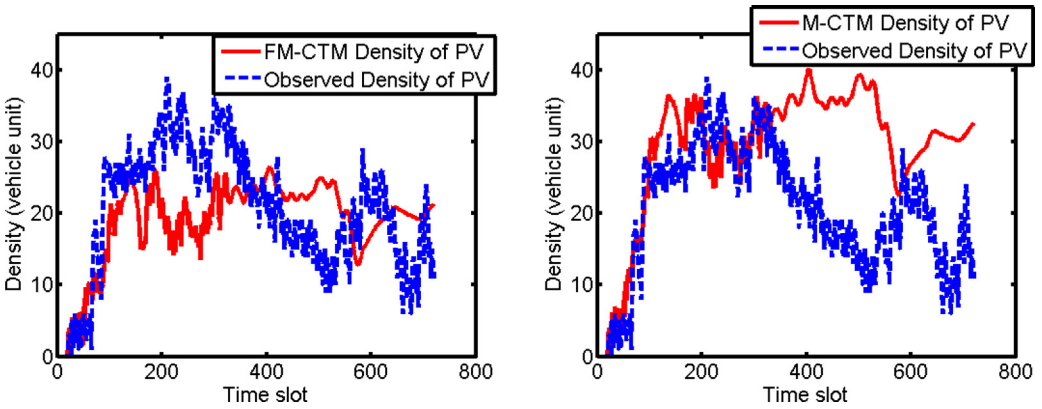

(a) FM-CTM (b) M-CTM

Fig. 12. Case 2: The comparison of of PV density history of cell 20.

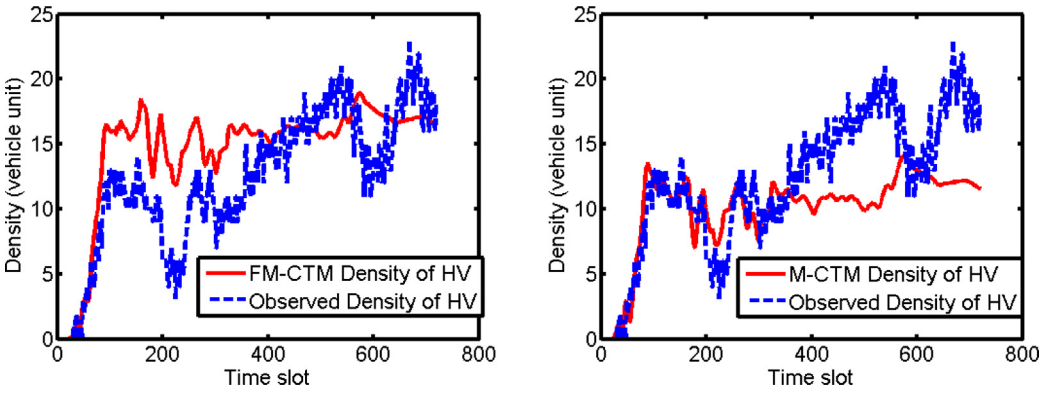

(a) FM-CTM (b) M-CTM

Fig. 13. Case 2: The comparison of of HV density history of cell 20.

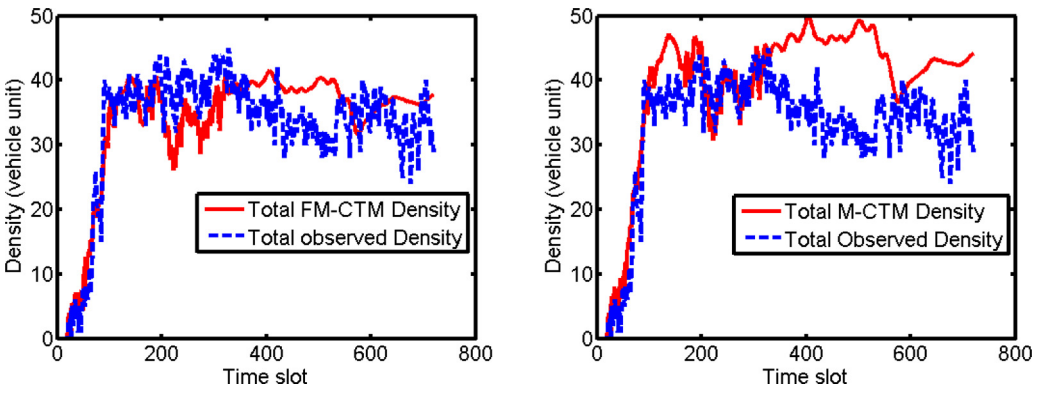

(a) FM-CTM (b) M-CTM

Fig. 14. Case 2: The comparison of total density history of cell 20.

Figs. 15–17 depict the evolution of traffic states of cell densities for case 2. M-CTM and M-CTM's total densities estimation are similar. However, FM-CTM can estimate PVs' and HVs' densities more accurate than M-CTM. M-CTM tends to overestimate PVs' densities, and, in turn, underestimate HVs' densities of cell 20. On the other hand, FM-CTM can track PVs' and HVs' densities of cell 20 better due to $\lambda_{link21,PV}$ allowing FM-CTM to better capture the dynamic of PVs' and HVs' densities and flows at the bottleneck between cells 20 and 21.

4.3. Case 3: Real road network of I-80

For case 3, the real traffic data was obtained from Next Generation Simulation (NGSIM) project (Federal Highway Administration, December 2006). The site is a segment of Interstate 80 in Emeryville (San Francisco), collected between 4:00 p.m. and 4:15 p.m., 5:00 p.m. and 5:15 p.m., and 5:15 p.m. and 5:30 p.m. The segment is about 400 m and with 6 lanes. The overall percentage of HVs is 5%. However, only the vehicle trajectory data between 4:00 p.m. and 4:15 p.m. were reconstructed over 15 min (Punzo et al., 2011; Montanino and Punzo, 2015). Thus, the data between 4.00 p.m. and 4.15 p.m. were

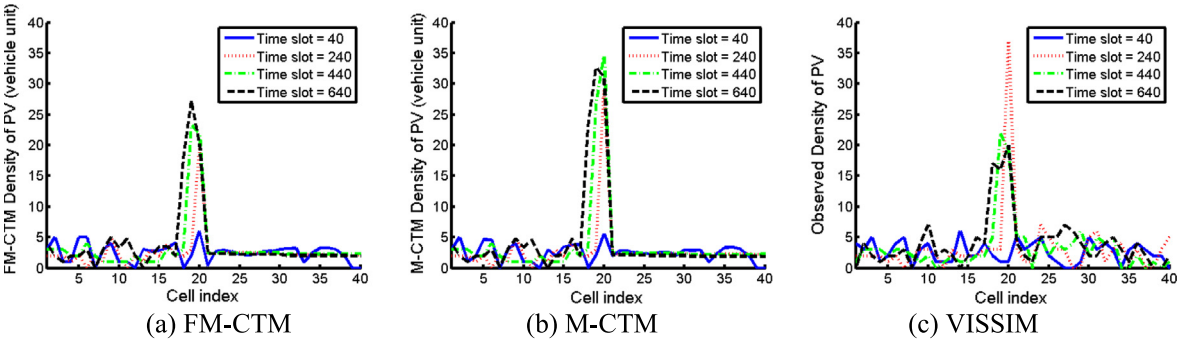

Fig. 15. Case 2: Comparison of density of PV for time slot 40, 240, 440, and 640.

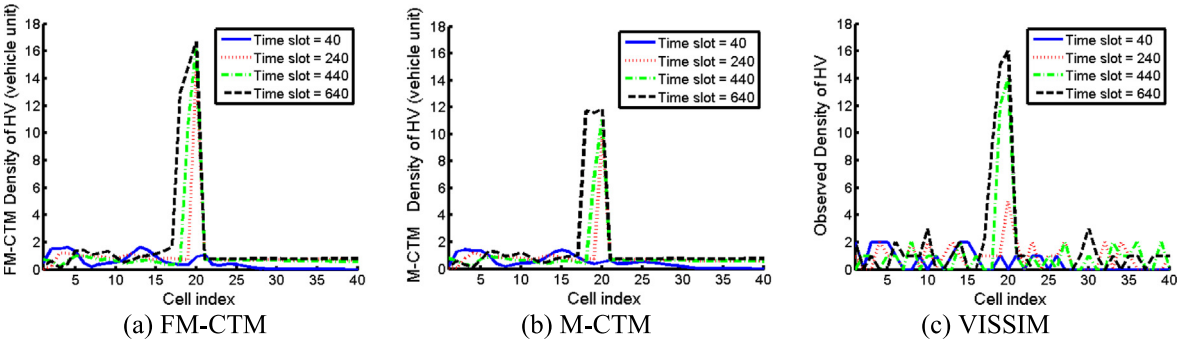

Fig. 16. Case 2: Comparison of density of HV for time slot 40, 240, 440, and 640.

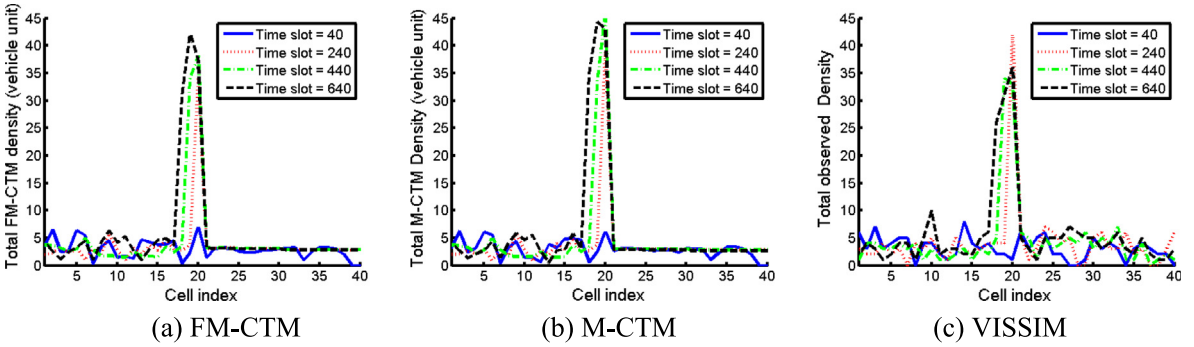

Fig. 17. Case 2: Comparison of density of Total density for time slot 40, 240, 440, and 640.

selected to evaluate the accuracy of FM-CTM. To avoid data deficiency at both ends of the segment and at the beginning and ending of recording time, only 360-m long segment and 860-s data of this period are selected for the evaluation.

The most-left lane is a high-occupancy vehicle (HOV) lane. From our observation, the traffic condition and vehicle speed of the HOV lane is drastically different from the rest, and there is little interaction between vehicles in the HOV lane and others. Therefore, we exclude this lane and its vehicle data from the experiment. There is also an on-ramp flow to the right-most lane near the boundary entry, which is approximated to be boundary entry flow to the first cell.

Time interval is 2 s with 430 total time slots. The densities of two vehicle classes, PVs and HVs, of each cell along with the boundary conditions are obtained from the vehicle trajectory data. The length of a PV, from the data, is 4.3 m. On the other hand, the length of an HV varies between 6.4 and 23 m. Here, we use the average length, 14 m, as HVs' length. Thus, the lower bounds of l_{PV} and l_{HV} are set to 4.3 and 14 m. Since the traffic is in congested condition, it is hard to accurately estimate free-flow speeds of PVs and HVs from the vehicle trajectory data. We estimated the free-flow speed from the speed limit. According to Deardoff et al. (2011), the possible range of the observed free-flow speed for the posted speed limit 105 km/h is between 80 and 130 km/h. We used 80 and 130 km/h as lower and upper bounds to manually calibrate the free-flow speed for CTMs. The manual calibration is basically trial and error as we re-process vehicle trajectory data to cell-based density data for a pre-determined free-flow speed then calibrates the other parameters with genetic algorithm to obtain the results for all CTMs. The free-flow speed of 82 km/h is found to be the most suitable as the densities estimations from CTMs are most accurate and able to track the traffic dynamic. The free-flow speed of HV is estimated to be 73% of PV's free-flow speed. Thus, the free-flow speed of PV and HV are estimated to be 23 and 17 m per second. The road segment is divided into 8 cells of 46-m length, as shown in Fig. 7.

From Table 5, FM-CTM shows an improvement over M-CTM by 15%. The resultant PV and HV' density comparisons of cells 4 and 8 are shown in Figs. 18–21. FM-CTM estimates PV's densities more accurately by taking into account the saturated condition in Eq. (10). On the other hand, M-CTM overestimated PVs' mobility in saturated condition because M-CTM did not consider that PVs were slowed down by HVs but assumed all vehicle classes run at their free-flow speed until congested condition.

For HV, FM-CTM and M-CTM' accuracies were the same. However, FM-CTM tended to overestimate HVs' densities while M-CTM did the opposite. FM-CTM estimated HV more accurately than M-CTM in cell 4 but less accurately in cell 8. Like in case 2, FM-CTM did not show improvement in terms of RMSE of HV because traffic condition is between saturated and congested where the difference between transmission functions of FM-CTM and M-CTM are minimal. Moreover, there is only 5% of HVs. and the impact of HV class is, therefore, relatively minor compared to the other two cases that have higher percentages of HVs Nonetheless, the impract of HVs to PVs were taken into account by both FM-CTM and M-CTM.

4.4. Comparison with S-CTM

In addition to the comparisons of $RMSE_{total}$ between FM-CTM and M-CTM, the conventional *RMSE* comparisons among FM-CTM, M-CTM, and S-CTM are provided in Table 6 for cases 1, 2, and 3. S-CTM is calibrated with the conventional RMSE as the fitness function. The calibration procedure of S-CTM is carried out in the same way as FM-CTM and M-CTM excluding their multiclass parameters such as class-specific parameters.

Even though both FM-CTM and M-CTM do not use the conventional RMSE as the fitness function, both still have lower RMSEs than S-CTM's. Again, FM-CTM still shows the superiority over M-CTM and S-CTM with its combination of FIFO and platoon dispersion properties. This implies, in order to estimate the traffic state well in various traffic conditions and physical

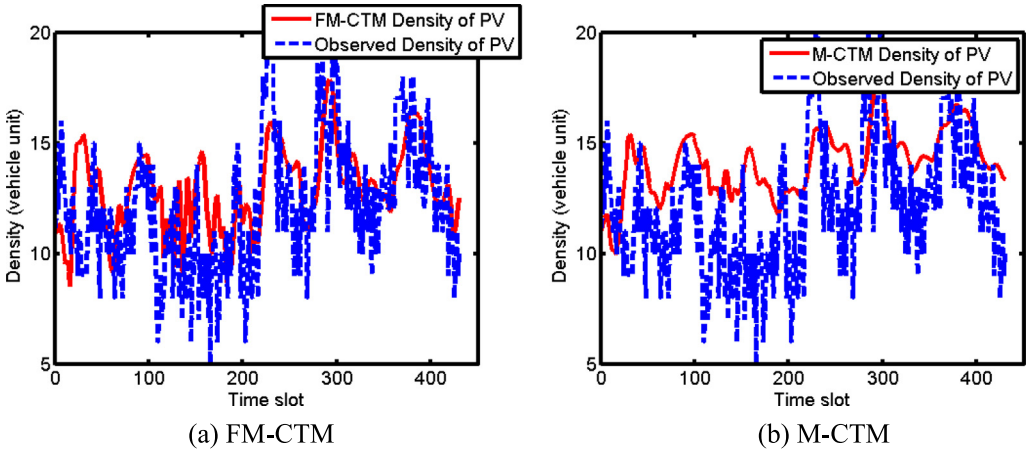

Fig. 18. Case 3: The comparison of of PV density history of cell 4.

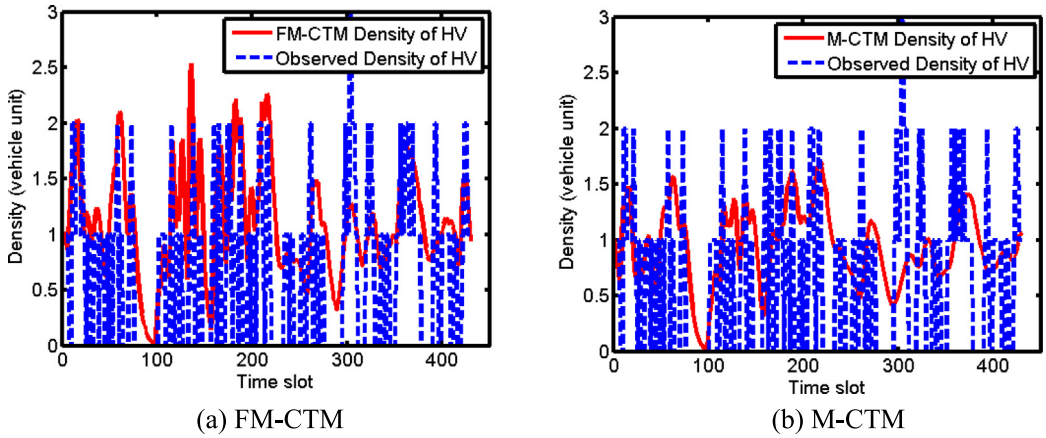

Fig. 19. Case 3: The comparison of of HV density history of cell 4.

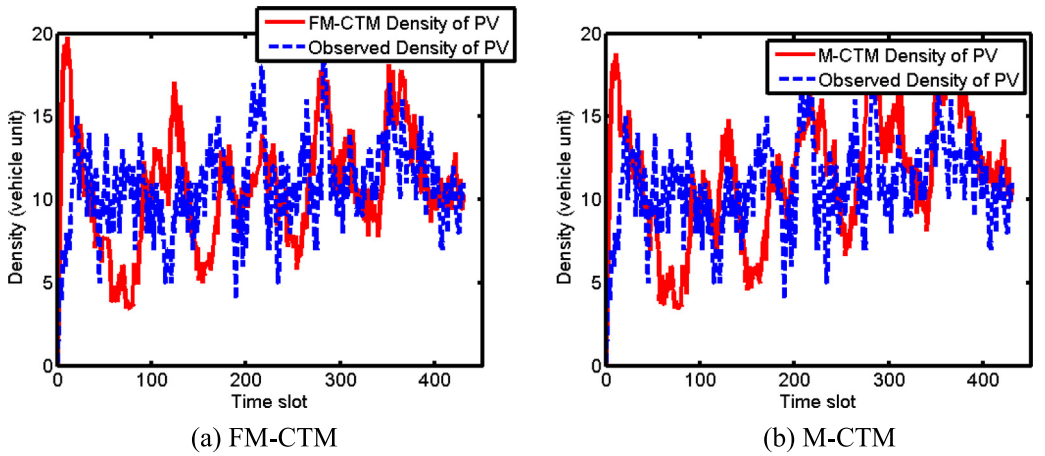

Fig. 20. Case 3: The comparison of of PV density history of cell 8.

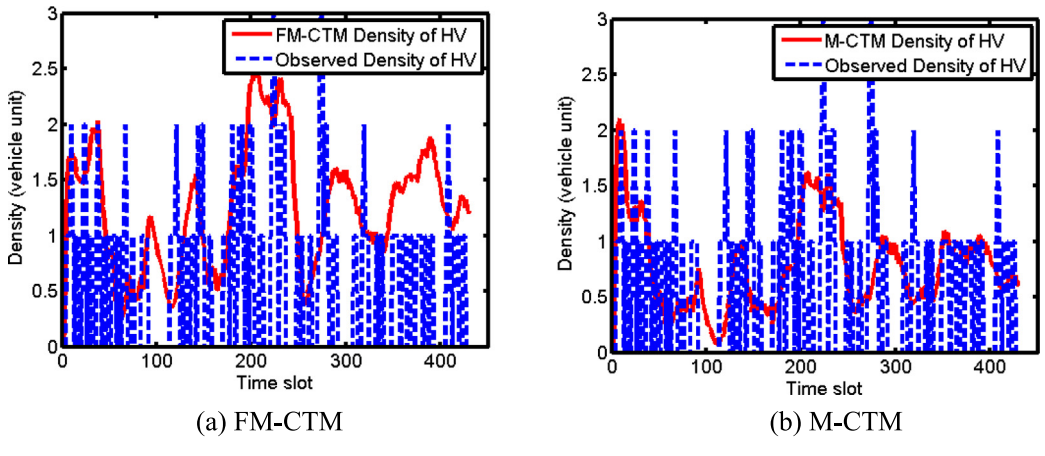

Fig. 21. Case 3: The comparison of of HV density history of cell 8.

lanes, multiclass macroscopic model should be able to identify the traffic conditions from multiclass state variables and correctly apply either FIFO or platoon dispersion model accordingly.

Table 6
The conventional RMSEs for FM-CTM, M-CTM, and S-CTM.

Case	FM-CTM's RMSE	M-CTM's RMSE	S-CTM's RMSE
1	1.34	1.56	2.07
2	2.22	2.64	5.15
3	2.98	3.78	5.71

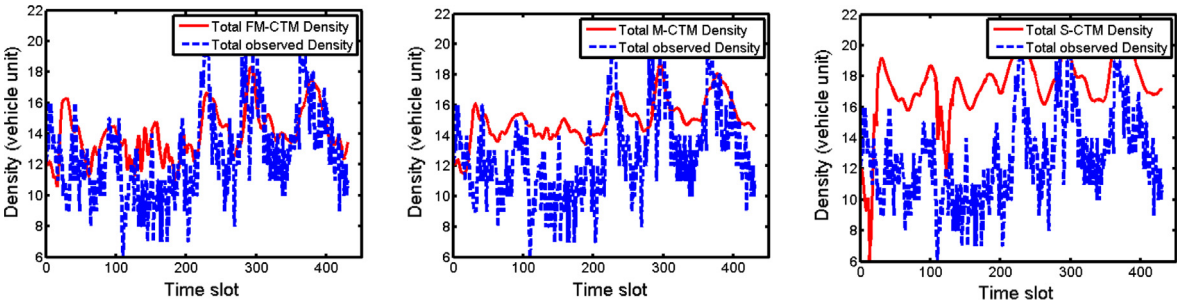

Fig. 22. Case 3: The comparison of FM-CTM, M-CTM, and S-CTM's total densities history of cell 4.

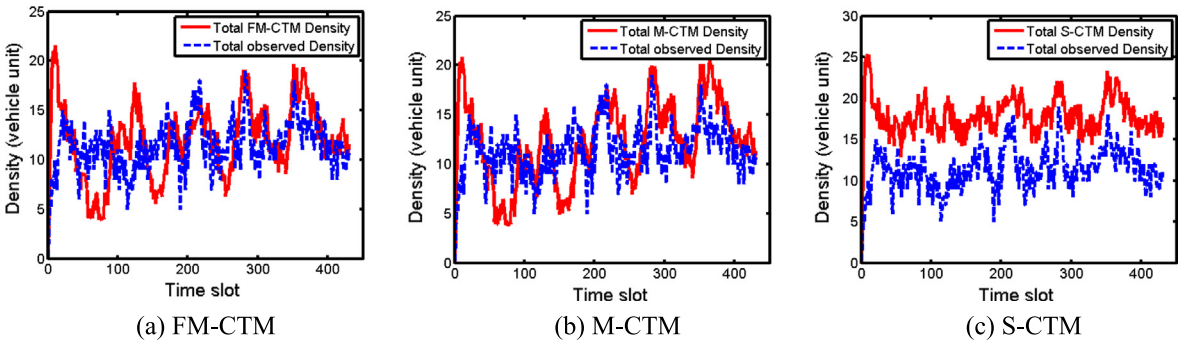

Fig. 23. Case 3: The comparison of FM-CTM, M-CTM, and S-CTM's total densities of cell 8.

The comparsion of total density in case 3 are shown in Figs. 22–24. In case 3, most of S-CTM's high RMSE comes from overestimating density. The cause is the imbalance of the actual boundary flow exit and the simulated incoming flow to the last cell. The reason is that S-CTM fails to take into account a minimum gap between vehicles, the longer length of HV, and the flow interruption by a slower HV. As a result, the flow estimated by S-CTM is much greater than FM-CTM flow and the actual flow and causes a queue propagating backward near the end of simulation. On the other hand, the incoming flow estimated by FM-CTM is more consistent with the actual flow and the boundary exit flow from the real-world data. This enables FM-CTM to track the dynamic of the last cell's density more accurately. While M-CTM can take into account some multiclass effects, M-CTM still fails to realize the PV's mobility drop since PVs share the road with HVs in saturated condition.

5. Conclusions

This paper is concerned with multiclass macroscopic modeling with FIFO property, FM-CTM for the cell-cascading scenario. The objective is to further enhance a well-established M-CTM to take into account FIFO property and the effect of lanes on platoon dispersion and FIFO property. Moreover, FM-CTM is further formulated to closed-form matrix equations. Theoretical proof shows that FM-CTM converges to the single-class LWR model. Based on the numerical results in two hypothetical freeway road networks and the real-world data, the closed-form FM-CTM has been validated to be more accurate than M-CTM with and without FIFO presented in the networks by 9–15% in terms of the RMSE of density, by estimating incoming flow more accurately than M-CTM. Like M-CTM, the closed-form FM-CTM can produce complicate phenomena such as platoon dispersion when lane changing and overtaking are available. For a case of a single lane, unlike M-CTM, FM-CTM enforces FIFO property to all vehicles, regardless of their free-flow speed. As a result, FM-CTM is more accurate than M-CTM in a road network with varying number of lanes. Therefore, the closed-form FM-CTM is expected to be applicable in practice. The

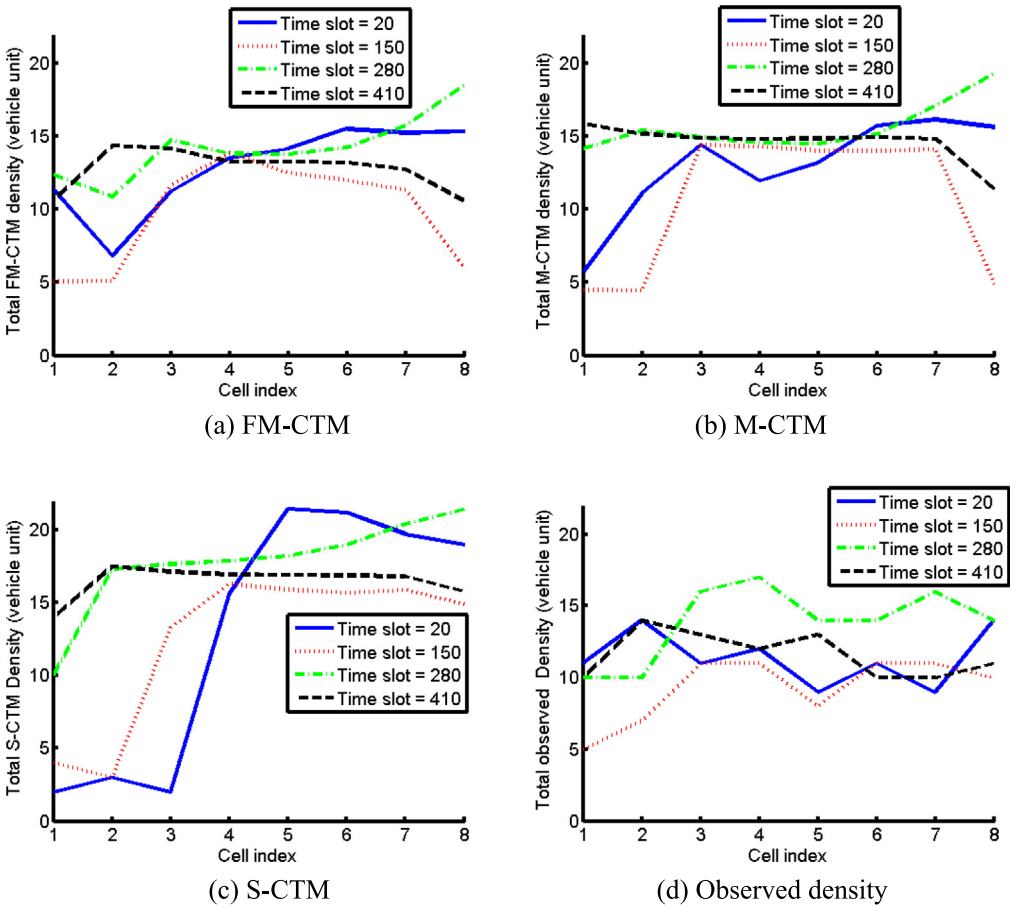

Fig. 24. Case 3: Comparison of FM-CTM, M-CTM, S-CTM, and total observed densities for time slot 20, 60, 100, and 140.

ongoing future work is to extend the closed-form FM-CTM to other two scenarios, merging and diverging, so that the model can be applied for a signalized intersection. The other is to take into account the effect of motorcycles in urban areas of a developing country.

Appendix A

A.1. The general closed-form FM-CTM

This section is to find the general closed-form for cascading scenario. The closed form is obtained by considering two parts separately: the head-of-cell flow and the end-of cell flow. We begin by proving the closed form of head-of-cell flow by proving Lemmas 1 and 2.

Lemma 1.

$$a_{i,m}(t) \geqslant \frac{\lambda_{i+1,m} a_{i,m}(t)\tilde{r}_{i+1}(t)}{\sum_{m=1}^{M}[\lambda_{i+1,m}\tilde{l}_m a_{i,m}(t)]} \rightarrow y_{i+1,m,a}(t) = \frac{\lambda_{i+1,m} a_{i,m}(t)\tilde{r}_{i+1}(t)}{\sum_{m=1}^{M}[\lambda_{i+1,m}\tilde{l}_m a_{i,m}(t)]}$$

Lemma 2.

$$a_{i,m}(t) \leqslant \frac{\lambda_{i+1,m} a_{i,m}(t)\tilde{r}_{i+1}(t)}{\sum_{m=1}^{M}[\lambda_{i+1,m}\tilde{l}_m a_{i,m}(t)]} \rightarrow y_{i+1,m,a}(t) = a_{i,m}(t)$$

Proof of Lemmas 1 and 2. The following sub lemmas first need to be proved.

Lemma 1.1 $\sum_{m=1}^{M}[l_m a_{i,m}(t)] \geqslant \tilde{r}_{i+1}(t) \leftrightarrow a_{i,m}(t) \geqslant \frac{\lambda_{i+1,m} a_{i,m}(t)\tilde{r}_{i+1}(t)}{\sum_{m=1}^{M}[\lambda_{i+1,m}\tilde{l}_m a_{i,m}(t)]}$

Lemma 2.1 $\sum_{m=1}^{M}[l_m a_{i,m}(t)] \leqslant \tilde{r}_{i+1}(t) \leftrightarrow a_{i,m}(t) \leqslant \frac{\lambda_{i+1,m} a_{i,m}(t)\tilde{r}_{i+1}(t)}{\sum_{m=1}^{M}[\lambda_{i+1,m}\tilde{l}_m a_{i,m}(t)]}$

Lemma 1.1 is proved if statements (A1) and (A2) are true:

$$\sum_{m=1}^{M}[l_m a_{i,m}(t)] \geqslant \tilde{r}_{i+1}(t) \rightarrow a_{i,m}(t) \geqslant \frac{\lambda_{i+1,m} a_{i,m}(t)\tilde{r}_{i+1}(t)}{\sum_{m=1}^{M}[\lambda_{i+1,m}\tilde{l}_m a_{i,m}(t)]} \tag{A1}$$

$$a_{i,m}(t) \geqslant \frac{\lambda_{i+1,m} a_{i,m}(t)\tilde{r}_{i+1}(t)}{\sum_{m=1}^{M}[\lambda_{i+1,m}\tilde{l}_m a_{i,m}(t)]} \rightarrow \sum_{m=1}^{M}[l_m a_{i,m}(t)] \geqslant \tilde{r}_{i+1}(t) \tag{A2}$$

From $a_{i,m}(t) < \frac{\lambda_{i+1,m} a_{i,m}(t)\tilde{r}_{i+1}(t)}{\sum_{m=1}^{M}[\lambda_{i+1,m}\tilde{l}_m a_{i,m}(t)]}$, multiply both sides by $\tilde{l}_m$ and take summation over m, we obtain $\sum_{m=1}^{M}[l_m a_{i,m}(t)] < \tilde{r}_{i+1}(t)$. Hence,

$$a_{i,m}(t) < \frac{\lambda_{i+1,m} a_{i,m}(t)\tilde{r}_{i+1}(t)}{\sum_{m=1}^{M}[\lambda_{i+1,m}\tilde{l}_m a_{i,m}(t)]} \rightarrow \sum_{m=1}^{M}[l_m a_{i,m}(t)] < \tilde{r}_{i+1}(t) \tag{A3}$$

Since $p \rightarrow q \equiv \sim q \rightarrow \sim p$, Eq. (A3) becomes

$$\sum_{m=1}^{M}[l_m a_{i,m}(t)] \geqslant \tilde{r}_{i+1}(t) \rightarrow a_{i,m}(t) \geqslant \frac{\lambda_{i+1,m} a_{i,m}(t)\tilde{r}_{i+1}(t)}{\sum_{m=1}^{M}[\lambda_{i+1,m}\tilde{l}_m a_{i,m}(t)]} \tag{A4}$$

Eq. (A4) is equivalent to statement (A1), thus the first statement is proved.

Proof of the second statement (A2), from $a_{i,m}(t) \geqslant \frac{\lambda_{i+1,m} a_{i,m}(t)\tilde{r}_{i+1}(t)}{\sum_{m=1}^{M}[\lambda_{i+1,m}\tilde{l}_m a_{i,m}(t)]}$, multiply both sides by $\tilde{l}_m$ and take summation over m, we obtain $\sum_{m=1}^{M}[l_m a_{i,m}(t)] \geqslant \tilde{r}_{i+1}(t)$. Therefore, the second statement is proved.

With the two statements being proved, Lemma 1.1 is proved. Lemma 2.1 can be proved in the similar way as Lemma 1.1 so the proof for Lemma 2.1 is omitted.

Lemmas 1.1 and 2.1 indicate that a comparison between a total sending capability of the beginning cell and the relative receiving capability is equivalent to a comparison between a head-of-cell vehicle and the allocated relative receiving capability for each class. Next, consider statement (A5):

$$\sum_{m=1}^{M}[\tilde{l}_m a_{i,m}(t)] > \tilde{r}_{i+1}(t) \rightarrow y_{i+1,m,a}(t) = \frac{\lambda_{i+1,m} a_{i,m}(t)\tilde{r}_{i+1}(t)}{\sum_{m=1}^{M}[\lambda_{i+1,m} l_m a_{i,m}(t)]} \tag{A5}$$

Statement (A5) is obtained from Eq. (3), from the fact that if there is not enough free space for the head-of-line vehicles then all the head-of-line vehicles from the upstream cell cannot advance to the downstream cell. The number of total vehicles that can advance to the downstream cell equals to the remaining space. Since $\sum_{m=1}^{M}[l_m a_{i,m}(t)] \geqslant \tilde{r}_{i+1}(t) \leftrightarrow a_{i,m}(t) \geqslant \frac{\lambda_{i+1,m} a_{i,m}(t)\tilde{r}_{i+1}(t)}{\sum_{m=1}^{M}[\lambda_{i+1,m}\tilde{l}_m a_{i,m}(t)]}$ from Lemma 1.1, statement (A6) is proved:

$$a_{i,m}(t) \geqslant \frac{\lambda_{i+1,m} a_{i,m}(t)\tilde{r}_{i+1}(t)}{\sum_{m=1}^{M}[\lambda_{i+1,m}\tilde{l}_m a_{i,m}(t)]} \rightarrow y_{i+1,m,a}(t) = \frac{\lambda_{i+1,m} a_{i,m}(t)\tilde{r}_{i+1}(t)}{\sum_{m=1}^{M}[\lambda_{i+1,m} l_m a_{i,m}(t)]} \tag{A6}$$

Thus, Lemma 1 is proved.

Proof of Lemma 2, consider statement (A7)

$$\sum_{m=1}^{M}[l_m a_{i,m}(t)] \leqslant \tilde{r}_{i+1}(t) \rightarrow y_{i+1,m,a}(t) = a_{i,m}(t) \tag{A7}$$

Statement (A7) is obtained from Eq. (2), from the fact that if there is enough free space for the head-of-line vehicles then all head-of-line vehicles from the upstream cell can forward to the downstream cell. Since $\sum_{m=1}^{M}[l_m a_{i,m}(t)] \leqslant \tilde{r}_{i+1}(t) \leftrightarrow a_{i,m}(t) \leqslant \frac{\lambda_{i+1,m} a_{i,m}(t)\tilde{r}_{i+1}(t)}{\sum_{m=1}^{M}[\lambda_{i+1,m}\tilde{l}_m a_{i,m}(t)]}$ from Lemma 2.1, Eq. (A7) becomes

$$a_{i,m}(t) \leqslant \frac{\lambda_{i+1,m} a_{i,m}(t)\tilde{r}_{i+1}(t)}{\sum_{m=1}^{M}[\lambda_{i+1,m}\tilde{l}_m a_{i,m}(t)]} \rightarrow y_{i+1,m,a}(t) = a_{i,m}(t) \tag{A8}$$

Thus, Lemma 2 is proved.

From Lemmas 1 and 2, the closed-form FM-CTM equation for head-of-cell flow is obtained.

$$y_{i+1,m,a}(t) = \min\left\{a_{i,m}(t), \frac{\lambda_{i+1,m} a_{i,m}(t)\tilde{r}_{i+1}(t)}{\sum_{m=1}^{M}[\lambda_{i+1,m} l_m a_{i,m}(t)]}\right\} \tag{A9}$$

Next, the closed form of the end-of-cell flow is obtained proving by the following three lemmas

Lemma 3. $\frac{\Gamma_{i,m}(t)b_{i,m}(t)\tilde{r}^*_{i+1}(t)}{\sum_{m=1}^{M}[\Gamma_{i,m}(t)l_m b_{i,m}(t)]} \leqslant 0 \rightarrow y_{i,m,b}(t) = 0$

Lemma 4. $0 \leqslant \frac{\Gamma_{i,m}(t)b_{i,m}(t)\tilde{r}^*_{i+1}(t)}{\sum_{m=1}^{M}[\Gamma_{i,m}(t)l_m b_{i,m}(t)]} \leqslant \Gamma_{i,m}(t)b_{i,m}(t) \rightarrow y_{i+1,m,b}(t) = \frac{\Gamma_{i,m}(t)b_{i,m}(t)\tilde{r}^*_{i+1}(t)}{\sum_{m=1}^{M}[\Gamma_{i,m}(t)l_m b_{i,m}(t)]}$

Lemma 5. $\frac{\Gamma_{i,m}(t)b_{i,m}(t)\tilde{r}^*_{i+1}(t)}{\sum_{m=1}^{M}[\Gamma_{i,m}(t)l_m b_{i,m}(t)]} \geqslant \Gamma_{i,m}(t)b_{i,m}(t) \rightarrow y_{i+1,m,b}(t) = \Gamma_{i,m}(t)b_{i,m}(t)$

Proof of Lemmas 3, 4 and 5. The following sub lemmas need to be proved.

Lemma 3.1 $\tilde{r}^*_{i+1}(t) \leqslant 0 \leftrightarrow \frac{\Gamma_{i,m}(t)b_{i,m}(t)\tilde{r}^*_{i+1}(t)}{\sum_{m=1}^{M}[\Gamma_{i,m}(t)l_m b_{i,m}(t)]} \leqslant 0.$

Lemma 4.1. $0 \leqslant \tilde{r}^*_{i+1}(t) \leqslant \sum_{m=1}^{M}[\Gamma_{i,m}(t)l_m b_{i,m}(t)] \leftrightarrow 0 \leqslant \frac{\Gamma_{i,m}(t)b_{i,m}(t)\tilde{r}^*_{i+1}(t)}{\sum_{m=1}^{M}[\Gamma_{i,m}(t)l_m b_{i,m}(t)]} \leqslant \Gamma_{i,m}(t)b_{i,m}(t)$

Lemma 5.1. $\tilde{r}^*_{i+1}(t) \geqslant \sum_{m=1}^{M}[\Gamma_{i,m}(t)l_m b_{i,m}(t)] \leftrightarrow \frac{\Gamma_{i,m}(t)b_{i,m}(t)\tilde{r}^*_{i+1}(t)}{\sum_{m=1}^{M}[\Gamma_{i,m}(t)l_m b_{i,m}(t)]} \geqslant \Gamma_{i,m}(t)b_{i,m}(t)$

Prove Lemma 3.1. Since $\Gamma_{i,m}(t)$ and $b_{i,m}(t)$ are non-negative for $\forall i, m$ and $\tilde{r}^*_{i+1}(t) \leqslant 0$, we can conclude that $\frac{\Gamma_{i,m}(t)b_{i,m}(t)\tilde{r}^*_{i+1}(t)}{\sum_{m=1}^{M}[\Gamma_{i,m}(t)l_m b_{i,m}(t)]} \leqslant 0$. As a result, Lemma 3.1 is proved.

Lemma 4.1 is proved by proving the two statements (A10) and (A11):

$$0 < \tilde{r}^*_{i+1}(t) \leqslant \sum_{m=1}^{M}[\Gamma_{i,m}(t)l_m b_{i,m}(t)] \rightarrow 0 < \frac{\Gamma_{i,m}(t)b_{i,m}(t)\tilde{r}^*_{i+1}(t)}{\sum_{m=1}^{M}[\Gamma_{i,m}(t)l_m b_{i,m}(t)]} \leqslant \Gamma_{i,m}(t)b_{i,m}(t) \tag{A10}$$

$$0 < \frac{\Gamma_{i,m}(t)b_{i,m}(t)\tilde{r}^*_{i+1}(t)}{\sum_{m=1}^{M}[\Gamma_{i,m}(t)l_m b_{i,m}(t)]} \leqslant \Gamma_{i,m}(t)b_{i,m}(t) \rightarrow 0 < \tilde{r}^*_{i+1}(t) \leqslant \sum_{m=1}^{M}[\Gamma_{i,m}(t)l_m b_{i,m}(t)] \tag{A11}$$

From inequality on the left hand of the statement (A10):

$$0 < \tilde{r}^*_{i+1}(t) \leqslant \sum_{m=1}^{M}[\Gamma_{i,m}(t)l_m b_{i,m}(t)] \tag{A12}$$

Because $\Gamma_{i,m}(t)b_{i,m}(t)$ is non-negative for $\forall m$, then $\frac{\Gamma_{i,m}(t)b_{i,m}(t)}{\sum_{m=1}^{M}[\Gamma_{i,m}(t)l_m b_{i,m}(t)]} > 0$ for $\forall m$. Multiply inequality (A12) with $\frac{\Gamma_{i,m}(t)b_{i,m}(t)}{\sum_{m=1}^{M}[\Gamma_{i,m}(t)l_m b_{i,m}(t)]}$, the inequality (A13) is obtained

$$0 < \frac{\Gamma_{i,m}(t)b_{i,m}(t)\tilde{r}^*_{i+1}(t)}{\sum_{m=1}^{M}[\Gamma_{i,m}(t)l_m b_{i,m}(t)]} \leqslant \Gamma_{i,m}(t)b_{i,m}(t) \tag{A13}$$

As a result, the first statement, Eq. (A10), is proved.

Then multiply inequality (A13) with l_m and sum over m, we obtain $0 < \tilde{r}^*_{i+1}(t) \leqslant \sum_{m=1}^{M}[\Gamma_{i,m}(t)l_m b_{i,m}(t)]$. Thus, the statement (A11) is proved. As a result, Lemma 4.1 is proved.

Prove Lemma 5.1. We have to prove the two statements (A14) and (A15)

$$\tilde{r}^*_{i+1}(t) \geqslant \sum_{m=1}^{M}[\Gamma_{i,m}(t)l_m b_{i,m}(t)] \rightarrow \frac{\Gamma_{i,m}(t)b_{i,m}(t)\tilde{r}^*_{i+1}(t)}{\sum_{m=1}^{M}[\Gamma_{i,m}(t)l_m b_{i,m}(t)]} \geqslant \Gamma_{i,m}(t)b_{i,m}(t) \tag{A14}$$

$$\frac{\Gamma_{i,m}(t)b_{i,m}(t)\tilde{r}^*_{i+1}(t)}{\sum_{m=1}^{M}[\Gamma_{i,m}(t)l_m b_{i,m}(t)]} \geqslant \Gamma_{i,m}(t)b_{i,m}(t) \rightarrow \tilde{r}^*_{i+1}(t) \geqslant \sum_{m=1}^{M}[\Gamma_{i,m}(t)l_m b_{i,m}(t)] \tag{A15}$$

From inequality of the left side of the statement (A14)

$$\tilde{r}^*_{i+1}(t) \geqslant \sum_{m=1}^{M}[\Gamma_{i,m}(t)l_m b_{i,m}(t)] \tag{A16}$$

Because $\Gamma_{i,m}(t)b_{i,m}(t)$ is non-negative for $\forall m$, $\frac{\Gamma_{i,m}(t)b_{i,m}(t)}{\sum_{m=1}^{M}[\Gamma_{i,m}(t)l_m b_{i,m}(t)]}$ is non-negative for $\forall m$. Multiply inequality (A16) with $\frac{\Gamma_{i,m}(t)b_{i,m}(t)}{\sum_{m=1}^{M}[\Gamma_{i,m}(t)l_m b_{i,m}(t)]}$, the inequality (A17) is obtained

$$\frac{\Gamma_{i,m}(t)b_{i,m}(t)\tilde{r}^*_{i+1}(t)}{\sum_{m=1}^{M}[\Gamma_{i,m}(t)l_m b_{i,m}(t)]} \geqslant \Gamma_{i,m}(t)b_{i,m}(t) \tag{A17}$$

As a result, statement (A14) is proved.

From $\frac{\Gamma_{i,m}(t)b_{i,m}(t)\tilde{r}^*_{i+1}(t)}{\sum_{m=1}^{M}[\Gamma_{i,m}(t)l_m b_{i,m}(t)]} \geqslant \Gamma_{i,m}(t)b_{i,m}(t)$, multiply with l_m and sum over m, $\tilde{r}^*_{i+1}(t) \geqslant \sum_{m=1}^{M}[\Gamma_{i,m}(t)l_m b_{i,m}(t)]$ is obtained. Thus, the second statement (A15) is proved. As a result, Lemma 5.1 is proved.

Lemmas 3.1, 4.1, and 5.1 imply that, instead of looking at the receiving capability after receiving head-of-cell vehicles and the end-of-cell vehicles, we can determine the flow of end-of-cell vehicles by considering $\frac{\Gamma_{i,m}(t)b_{i,m}(t)\tilde{r}^*_{i+1}(t)}{\sum_{m=1}^{M}[\Gamma_{i,m}(t)l_m b_{i,m}(t)]}$ and $\Gamma_{i,m}(t)b_{i,m}(t)$. Combining cascading equations from FM-CTM and Lemmas 3.1, 4.1 and 5.1 allows us to obtain Lemmas 3–5 as follows:

Statement (A18) is obtained from Eq. (13). With statement (A18) and Lemma 3.1, we obtain statement (A19)

$$\tilde{r}^*_{i+1}(t) \leqslant 0 \rightarrow y_{i+1,m,b}(t) = 0 \tag{A18}$$

$$\frac{\Gamma_{i,m}(t)b_{i,m}(t)\tilde{r}^*_{i+1}(t)}{\sum_{m=1}^{M}[\Gamma_{i,m}(t)l_m b_{i,m}(t)]} \leqslant 0 \rightarrow y_{i+1,m,b}(t) = 0 \tag{A19}$$

Thus, Lemma 3 is proved.

Statement (A20) is obtained from Eqs. (15). With statement (A20) and Lemma 4.1, Lemma 4 is proved.

$$0 \leqslant \tilde{r}^*_{i+1}(t) \leqslant \sum_{m=1}^{M}[\Gamma_{i,m}(t)l_m b_{i,m}(t)] \rightarrow y_{i+1,m,b}(t) = \frac{\Gamma_{i,m}(t)b_{i,m}(t)\tilde{r}^*_{i+1}(t)}{\sum_{m=1}^{M}[\Gamma_{i,m}(t)l_m b_{i,m}(t)]} \tag{A20}$$

Statement (A21) is obtained from Eqs. (14). With statement (A21) and Lemma 5.1, Lemma 5 is proved.

$$\sum_{m=1}^{M}[\Gamma_{i,m}(t)b_{i,m}(t)] \leqslant \tilde{r}^*_{i+1}(t) \rightarrow y_{i+1,m,b}(t) = \Gamma_{i,m}(t)b_{i,m}(t) \tag{A21}$$

From Lemma 3–5, the closed-form FM-CTM equation for end-of-cell flow is obtained as in Eq. (A22):

$$y_{i+1,m,b}(t) = \text{median}\left\{0, \frac{\Gamma_{i,m}(t)b_{i,m}(t)\tilde{r}^*_{i+1}(t)}{\sum_{m=1}^{M}[\Gamma_{i,m}(t)l_m b_{i,m}(t)]}, \Gamma_{i,m}(t)b_{i,m}(t)\right\} \tag{A22}$$

Combine the end-of-cell flow from Eq. (A22) with the head-of-cell flow from Eq. (A9), the closed-form equation for calculating flow for FM-CTM is obtained

$$y_{i+1,m}(t) = \min\left\{a_{i,m}(t), \frac{\lambda_{i+1,m}a_{i,m}(t)\tilde{r}_{i+1}(t)}{\sum_{m=1}^{M}[\lambda_{i+1,m}l_m a_{i,m}(t)]}\right\} + \text{median}\left\{0, \frac{\Gamma_{i,m}(t)b_{i,m}(t)\tilde{r}^*_{i+1}(t)}{\sum_{m=1}^{M}[\Gamma_{i,m}(t)l_m b_{i,m}(t)]}, \Gamma_{i,m}(t)b_{i,m}(t)\right\} \tag{A23}$$

Rewritten Eq. (A23) in matrix form,

$$\vec{Y}_{i+1,a}(t) = \min\left\{\vec{A}_i(t), \frac{\tilde{r}_{i+1}(t)}{\vec{\lambda}_{i+1}{}^T diag(\vec{\tilde{L}})\vec{A}_i(t)} diag(\vec{\lambda}_{i+1})\vec{A}_i(t)\right\} \tag{A24}$$

$$\vec{Y}_{i+1,b}(t) = \text{median}\left\{\vec{0}_{M\times 1}, \frac{\tilde{r}^*_{i+1}(t)}{\vec{\Gamma}_i(t)^T diag(\vec{\tilde{L}})\vec{B}_i(t)} diag(\vec{\Gamma}_i(t))\vec{B}_i(t), diag(\vec{\Gamma}_i(t))\vec{B}_i(t)\right\} \tag{A25}$$

$$\vec{Y}_{i+1}(t) = \vec{Y}_{i+1,a}(t) + \vec{Y}_{i+1,b}(t) \tag{A26}$$

where

$$\vec{A}_i(t) = [a_{i,1}(t), \ldots, a_{i,M}(t)]^T, \vec{B}_i(t) = [b_{i,1}(t), \ldots, b_{i,M}(t)]^T, \vec{N}_{i+1}(t) = [n_{i+1,1}(t), \ldots, n_{i+1,M}(t)]^T,$$
$$\vec{Y}_{i+1,a}(t) = [y_{i+1,1,a}(t), \ldots, y_{i+1,M,a}(t)]^T, \vec{Y}_{i+1,b}(t) = [y_{i+1,1,b}(t), \ldots, y_{i+1,M,b}(t)]^T,$$

$$\vec{Y}_{i+1}(t) = [y_{i,1}(t), \ldots, y_{i,M}(t)]^T, \vec{\tilde{L}} = [\tilde{l}_1, \ldots, \tilde{l}_M]^T, \vec{\lambda}_{i+1} = [\lambda_{i+1,1}, \ldots, \lambda_{i+1,M}]^T,$$

$$\vec{\Gamma}_i(t) = [\Gamma_{i,1}(t), \ldots, \Gamma_{i,M}(t)]^T, diag(\vec{\lambda}_{i+1}) = \begin{bmatrix} \lambda_{i+1,1} & 0 & \cdots & 0 \\ 0 & \lambda_{i+1,2} & \cdots & 0 \\ \vdots & \vdots & \ddots & \vdots \\ 0 & 0 & \cdots & \lambda_{i+1,M} \end{bmatrix}$$

$$diag(\vec{\Gamma}_i(t)) = \begin{bmatrix} \Gamma_{i,1}(t) & 0 & \cdots & 0 \\ 0 & \Gamma_{i,2}(t) & \cdots & 0 \\ \vdots & \vdots & \ddots & \vdots \\ 0 & 0 & \cdots & \Gamma_{i,M}(t) \end{bmatrix},$$

$$diag(\vec{\tilde{L}}) = \begin{bmatrix} \tilde{l}_1 & 0 & \cdots & 0 \\ 0 & \tilde{l}_2 & \cdots & 0 \\ \vdots & \vdots & \ddots & \vdots \\ 0 & 0 & \cdots & \tilde{l}_M \end{bmatrix}$$

Obviously, when either or both $\vec{A}_i(t) = \vec{0}$ and $\vec{B}_i(t) = \vec{0}$, the denominator is zero and the ration becomes infinity. However, we know that when there is no head-of-cell vehicle in an upstream cell, the head-of-cell flow is zero. This is also true for an end-of-cell vehicle. As a result, the matrix flow equation above is for when $\vec{A}_i(t) \neq \vec{0}$ and $\vec{B}_i(t) \neq \vec{0}$. In case that either or both of them are $\vec{0}$, the respective flow of their type is $\vec{0}$ and further calculation using the flow equation for respective flow is not needed.

References

Alecsandru, C.D., 2006. A stochastic mesoscopic cell-transmission model for operational analysis of large-scale transportation networks.

Boel, R., Mihaylova, L., 2006. A compositional stochastic model for real time freeway traffic simulation. Transport. Res. Part B: Methodol. 40, 319–334.

Carey, M., Balijepalli, C., Watling, D., 2015. Extending the cell transmission model to multiple lanes and lane-changing. Networ. Spatial Econ. 15, 507–535.

Castillo, E., Grande, Z., Calviño, A., Szeto, W.Y., Lo, H.K., 2015. A state-of-the-art review of the sensor location, flow observability, estimation, and prediction problems in traffic networks. J. Sens.

Celikoglu, H.B., 2013. An approach to dynamic classification of traffic flow patterns. Comput. –Aid. Civil Infrastruct. Eng. 28, 273–288.

Celikoglu, H.B., 2014. Dynamic classification of traffic flow patterns simulated by a switching multimode discrete cell transmission model. IEEE Trans. Intell. Transp. Syst. 15, 2539–2550.

Celikoglu, H.B., Silgu, M.A., 2016. Extension of traffic flow pattern dynamic classification by a macroscopic model using multivariate clustering. Transport. Sci. 50, 966–981.

Daganzo, C.F., 1994. The cell transmission model: a dynamic representation of highway traffic consistent with the hydrodynamic theory. Transport. Res. Part B: Methodol. 28, 269–287.

Daganzo, C.F., 1995. The cell transmission model, part II: network traffic. Transport. Res. Part B: Methodol. 29, 79–93.

Daganzo, C.F., 1999. The lagged cell-transmission model.

Deardoff, M.D., Wiesner, B.N., Fazio, J., 2011. Estimating free-flow speed from posted speed limit signs. Procedia – Soc. Behav. Sci. 16, 306–316.

Federal highway administration, U. S. D. O. T. December 2006. Interstate 80 Freeway Dataset <https://www.fhwa.dot.gov/publications/research/operations/06137/index.cfm>. Available: <https://www.fhwa.dot.gov/publications/research/operations/06137/index.cfm> [Accessed 31 April 2017].

Flötteröd, G., Nagel, K., 2005. Some practical extensions to the cell transmission model. In: ITSC 2005 8th International IEEE Conference on Intelligent Transportation Systems.

Gomes, G., Horowitz, R., 2006. Optimal freeway ramp metering using the asymmetric cell transmission model. Transport. Res. Part C: Emerg. Technol. 14, 244–262.

Gomes, G., Horowitz, R., Kurzhanskiy, A.A., Varaiya, P., Kwon, J., 2008. Behavior of the cell transmission model and effectiveness of ramp metering. Transport. Res. Part C: Emerg. Technol. 16, 485–513.

Hadfi, R., Tokuda, S., Ito, T., 2017. Traffic simulation in urban networks using stochastic cell transmission model. Comput. Intel.

Han, Y., Hegyi, A., Yuan, Y., Hoogendoorn, S., 2017. Validation of an extended discrete first-order model with variable speed limits. Transport. Res. Part C: Emerg. Technol. 83, 1–17.

Kalafatas, G., Peeta, S., 2010. A graph-based formulation for the multiple destinations dynamic traffic assignment problem. Chapters.

Laval, J.A., Daganzo, C.F., 2006. Lane-changing in traffic streams. Transport. Res. Part B: Methodol. 40, 251–264.

Levin, M.W., Boyles, S.D., 2016a. A cell transmission model for dynamic lane reversal with autonomous vehicles. Transport. Res. Part C: Emerg. Technol. 68, 126–143.

Levin, M.W., Boyles, S.D., 2016b. A multiclass cell transmission model for shared human and autonomous vehicle roads. Transport. Res. Part C: Emerg. Technol. 62, 103–116.

Lighthill, M.J., Whitham, G.B., 1955. On kinematic waves. II. A theory of traffic flow on long crowded roads. In: Proceedings of the Royal Society of London A: Mathematical, Physical and Engineering Sciences. The Royal Society, pp. 317–345.

Liu, H., Wang, J., Wijayaratna, K., Dixit, V.V., Waller, S.T., 2015. Integrating the bus vehicle class into the cell transmission model. IEEE Trans. Intell. Transp. Syst. 16, 2620–2630.

Lo, H.K., Chang, E., Chan, Y.C., 2001. Dynamic network traffic control. Transport. Res. Part A: Pol. Pract. 35, 721–744.

Lu, S., Dai, S., Liu, X., 2011. A discrete traffic kinetic model–integrating the lagged cell transmission and continuous traffic kinetic models. Transport. Res. Part C: Emerg. Technol. 19, 196–205.

Mesa-Arango, R., Ukkusuri, S.V., 2014. Modeling the car-truck interaction in a system-optimal dynamic traffic assignment model. J. Intel. Transport. Syst. 18, 327–338.

Mohan, R., Ramadurai, G., 2013. State-of-the art of macroscopic traffic flow modelling. Int. J. Adv. Eng. Sci. Appl. Math. 5, 158–176.

Montanino, M., Punzo, V., 2015. Trajectory data reconstruction and simulation-based validation against macroscopic traffic patterns. Transport. Res. Part B: Methodol. 80, 82–106.

Nair, R., Mahmassani, H.S., Miller-Hooks, E., 2011. A porous flow approach to modeling heterogeneous traffic in disordered systems. Procedia-Social Behav. Sci. 17, 611–627.

Ngoduy, D., 2011. Multiclass first-order traffic model using stochastic fundamental diagrams. Transportmetrica 7, 111–125.

Ngoduy, D., Liu, R., 2007. Multiclass first-order simulation model to explain non-linear traffic phenomena. Phys. A 385, 667–682.

Punzo, V., Borzacchiello, M.T., Ciuffo, B., 2011. On the assessment of vehicle trajectory data accuracy and application to the Next Generation SIMulation (NGSIM) program data. Transport. Res. Part C: Emerging Technol. 19, 1243–1262.

Qian, Z.S., Li, J., Li, X., Zhang, M., Wang, H., 2017. Modeling heterogeneous traffic flow: a pragmatic approach. Transport. Res. Part B: Methodol. 99, 183–204.

Richards, P.I., 1956. Shock waves on the highway. Operat. Res. 4, 42–51.

Silgu, M.A., Celikoglu, H.B., 2015. Clustering traffic flow patterns by Fuzzy C-means method: some preliminary findings. In: International Conference on Computer Aided Systems Theory. Springer, pp. 756–764.
Sumalee, A., Zhong, R., Pan, T., Szeto, W., 2011. Stochastic cell transmission model (SCTM): a stochastic dynamic traffic model for traffic state surveillance and assignment. Transport. Res. Part B: Methodol. 45, 507–533.
Szeto, W., 2008. Enhanced lagged cell-transmission model for dynamic traffic assignment. Transport. Res. Rec.: J. Transport. Res. Board, 76–85.
Szeto, W.Y., Jiang, Y., Sumalee, A., 2011. A cell-based model for multi-class doubly stochastic dynamic traffic assignment. Comput.-Aid. Civil Infrastruct. Eng. 26, 595–611.
Tuerprasert, K., Aswakul, C., 2010. Multiclass cell transmission model for heterogeneous mobility in general topology of road network. J. Intel. Transport. Syst. 14, 68–82.
Ukkusuri, S.V., Waller, S.T., 2008. Linear programming models for the user and system optimal dynamic network design problem: formulations, comparisons and extensions. Networks Spatial Econ. 8, 383–406.
Van Lint, J., Hoogendoorn, S., Schreuder, M., 2008. Fastlane: new multiclass first-order traffic flow model. Transport. Res. Rec.: J. Transport. Res. Board, 177–187.
Vissim, P., 2008. 5.10 User Manual. PTV Planung Transport Verkehr AG, Stumpfstraße, 1.
Wong, G., Wong, S., 2002. A multi-class traffic flow model – an extension of LWR model with heterogeneous drivers. Transport. Res. Part A: Policy Pract. 36, 827–841.
Work, D.B., Tossavainen, O.-P., Blandin, S., Bayen, A.M., Iwuchukwu, T., Tracton, K., 2008. An ensemble Kalman filtering approach to highway traffic estimation using GPS enabled mobile devices. In: Decision and Control, 2008. CDC 2008. 47th IEEE Conference on. IEEE. p. 5062–5068.
Zhan, X., Ukkusuri, S.V., 2017. Multiclass, simultaneous route and departure time choice dynamic traffic assignment with an embedded spatial queuing model. Transportmetrica B: Transport Dyn., 1–23
Zhang, L., Yin, Y., Chen, S., 2013. Robust signal timing optimization with environmental concerns. Transport. Res. Part C: Emerg. Technol. 29, 55–71.
Zhang, Z., Wolshon, B., Dixit, V.V., 2015. Integration of a cell transmission model and macroscopic fundamental diagram: network aggregation for dynamic traffic models. Transport. Res. Part C: Emerg. Technol. 55, 298–309.
Zhong, R., Sumalee, A., 2008. Stochastic cell transmission model: traffic state estimation under uncertainties. Traffic Transport. Stud.
Zhu, F., Lo, H.K., Lin, H.-Z., 2013. Delay and emissions modelling for signalised intersections. Transportmetrica B: Transp. Dyn. 1, 111–135.